$\Lambda_b \to \Lambda_c^*(2595, 2625)\ell^-\bar{\nu}$ form factors from lattice QCD

Stefan Meinel[1] and Gumaro Rendon[2]

[1]*Department of Physics, University of Arizona, Tucson, Arizona 85721, USA*
[2]*Physics Department, Brookhaven National Laboratory, Upton, New York 11973, USA*

(Received 22 March 2021; accepted 9 April 2021; published 24 May 2021)

We present the first lattice-QCD determination of the form factors describing the semileptonic decays $\Lambda_b \to \Lambda_c^*(2595)\ell^-\bar{\nu}$ and $\Lambda_b \to \Lambda_c^*(2625)\ell^-\bar{\nu}$, where the $\Lambda_c^*(2595)$ and $\Lambda_c^*(2625)$ are the lightest charm baryons with $J^P = \frac{1}{2}^-$ and $J^P = \frac{3}{2}^-$, respectively. These decay modes provide new opportunities to test lepton flavor universality and also play an important role in global analyses of the strong interactions in $b \to c$ semileptonic decays. We determine the full set of vector, axial vector, and tensor form factors for both decays but only in a small kinematic region near the zero-recoil point. The lattice calculation uses three different ensembles of gauge-field configurations with $2 + 1$ flavors of domain-wall fermions, and we perform extrapolations of the form factors to the continuum limit and physical pion mass. We present Standard Model predictions for the differential decay rates and angular observables. In the kinematic region considered, the differential decay rate for the $\frac{1}{2}^-$ final state is found to be approximately 2.5 times larger than the rate for the $\frac{3}{2}^-$ final state. We also test the compatibility of our form-factor results with zero-recoil sum rules.

DOI: 10.1103/PhysRevD.103.094516

I. INTRODUCTION

Semileptonic $b \to c\ell^-\bar{\nu}$ decays are used to determine the CKM matrix element V_{cb} and to search for deviations from lepton flavor universality [1–3]. They also provide an important testing ground for heavy-quark effective theory [4]. In recent years, the operation of the Large Hadron Collider has provided new opportunities for measurements involving b baryons. The simplest baryonic $b \to c\ell^-\bar{\nu}$ process is $\Lambda_b \to \Lambda_c\ell^-\bar{\nu}$, in which both the initial and final hadrons are the ground states with $J^P = \frac{1}{2}^+$. This mode has been used in combination with $\Lambda_b \to p\ell^-\bar{\nu}$ to determine $|V_{ub}/V_{cb}|$ [5,6] and offers the prospect of measuring the τ-versus-μ ratio $R(\Lambda_c)$ and related observables [2,3]. The baryonic decays can provide complementary information on physics beyond the Standard Model when compared with mesonic decays [7–17]. The $\Lambda_b \to \Lambda_c$ form factors have been computed using lattice QCD [5,10,18,19], and the lattice results predict a shape for the $\Lambda_b \to \Lambda_c\mu^-\bar{\nu}$ differential decay rate in the Standard Model that is consistent with the LHCb measurement [20]. Heavy-quark symmetry provides strong constraints on $\Lambda_b \to \Lambda_c\mu^-\bar{\nu}$, in which the light hadronic degrees of freedom have total angular momentum zero. In the heavy-quark-effective-theory (HQET) description of this decay, no subleading order-$\Lambda_{\rm QCD}/m_{c,b}$ Isgur-Wise functions occur and only two sub-subleading Isgur-Wise functions enter at order $\Lambda_{\rm QCD}^2/m_c^2$; the available lattice and LHCb results are well described by a fit of this order [21,22].

In addition to $\Lambda_b \to \Lambda_c\mu^-\bar{\nu}$, the LHCb detector has also collected (and will continue to collect) large numbers of $\Lambda_b \to \Lambda_c^*(2595)\mu^-\bar{\nu}$ and $\Lambda_b \to \Lambda_c^*(2625)\mu^-\bar{\nu}$ samples [20]. The $\Lambda_c^*(2595)$ and $\Lambda_c^*(2625)$ are the lightest charm baryons with $J^P = \frac{1}{2}^-$ and $J^P = \frac{3}{2}^-$, respectively, and are very narrow resonances decaying to $\Lambda_c\pi\pi$ [23]. It has been projected that $R(\Lambda_c^*) = \mathcal{B}(\Lambda_b \to \Lambda_c^*\tau^-\bar{\nu})/\mathcal{B}(\Lambda_b \to \Lambda_c^*\mu^-\bar{\nu})$ can be measured using LHCb data with approximately 17% uncertainty at the end of LHC Run 3, and as low as 5% uncertainty at the end of Run 6 [3]. To predict $R(\Lambda_c^*)$ in the Standard Model and beyond, the $\Lambda_b \to \Lambda_c^*$ form factors are needed. A calculation of these form factors may also improve the control of the backgrounds in a measurement of $R(\Lambda_c)$. Another potential impact will be on zero-recoil sum rules [24,25] and on global analyses of $b \to c\ell^-\bar{\nu}$ form factors using dispersion relations [26]. The authors of Ref. [26] wrote "Given the large fractional saturation of the unitarity bounds by $\Lambda_b \to \Lambda_c$, the inclusion of $\Lambda_b \to \Lambda_c^*$ could be particularly fruitful once such data is available." Finally, we note that there is significant interest in the structure and strong decays of the $\Lambda_c^*(2595)$ and $\Lambda_c^*(2625)$, in part due to the closeness of the $\Sigma_c^{(*)}\pi$ thresholds [27–31].

In the limit of heavy charm quarks, the light degrees of freedom in $\Lambda_c^*(2595)$ and $\Lambda_c^*(2625)$ have total angular

momentum 1 and these two baryons become degenerate. Note that there is no heavy-quark spin-symmetry relation between the Λ_c^* and the Λ_c due to the different quantum numbers of the light degrees of freedom. This difference also means that the normalization of the leading Isgur-Wise function for $\Lambda_b \to \Lambda_c^*$ remains unconstrained in the heavy-quark limit, and the matrix elements vanish at zero recoil [32,33]. The HQET relations for the $\Lambda_b \to \Lambda_c^*(2595)$ and $\Lambda_b \to \Lambda_c^*(2625)$ vector and axial vector form factors including the subleading order-$\Lambda_{\rm QCD}/m_{c,b}$ contributions were derived in Refs. [25,32,33]; the authors of the latter reference specifically studied the possibility of using HQET fits to LHCb data for the muonic decay $\Lambda_b \to \Lambda_c^* \mu^- \bar{\nu}$ to make Standard Model predictions for $R(\Lambda_c^*)$. It is still an open question how well HQET at this order can describe these transitions.

Quark-model studies of the $\Lambda_b \to \Lambda_c^*(2595)$ and $\Lambda_b \to \Lambda_c^*(2625)$ form factors can be found in Refs. [34–37]. In the following, we present the first lattice-QCD determination of these form factors. Our calculation follows that of the $\Lambda_b \to \Lambda^*(1520)$ form factors in Ref. [38] and uses the same ensembles of gauge-field configurations. We observe that the $\Lambda_c^*(2595)$ and $\Lambda_c^*(2625)$ energy levels for our simulation parameters are below all potential strong-decay thresholds, although they come quite close at the lowest pion mass. As in Ref. [38], we work in the rest frame of the final-state baryon to avoid mixing between $J = \frac{3}{2}$ and $J = \frac{1}{2}$ and between negative and positive parity. This again limits the kinematic coverage to the region near $q^2_{\rm max}$.

Our definitions of the form factors are given in Sec. II. Following a brief summary of the lattice parameters in Sec. III, we discuss the baryon interpolating fields, two-point functions, and the results for the masses in Sec. IV. The extraction of the form factors from three-point functions is described in Sec. V, and their extrapolation to the physical pion mass and continuum limit is discussed in Sec. VI. We test the compatibility with zero-recoil sum rules in Sec. VII and present the Standard Model predictions for $\Lambda_b \to \Lambda_c^*(2595)\ell^-\bar{\nu}$ and $\Lambda_b \to \Lambda_c^*(2625)\ell^-\bar{\nu}$ in Sec. VIII. Our conclusions are given in Sec. IX, and the Appendix contains relations to other form factor definitions used in the literature.

II. DEFINITIONS OF THE FORM FACTORS

In the following, we denote the $\Lambda_c^*(2595)$ and $\Lambda_c^*(2625)$ as $\Lambda_{c,1/2}^*$ and $\Lambda_{c,3/2}^*$, respectively. The masses and total decay widths determined by experiments are $m_{\Lambda_{c,1/2}^*} = 2592.25(28)$ MeV, $m_{\Lambda_{c,3/2}^*} = 2628.11(19)$ MeV, $\Gamma_{\Lambda_{c,1/2}^*} = 2.6(0.6)$ MeV, $\Gamma_{\Lambda_{c,3/2}^*} < 0.97$ MeV (CL = 90%) [23]. We neglect the decay widths throughout this work. In our lattice calculations at heavier-than-physical pion masses, the strong decays are in fact kinematically forbidden, except perhaps at the lightest pion mass; the hadron masses we find on the lattice are given in Sec. IV.

We normalize the baryon states as

$$\langle \Lambda_b(\mathbf{k}, r) | \Lambda_b(\mathbf{p}, s) \rangle = \delta_{rs} 2E_{\Lambda_b} (2\pi)^3 \delta^3(\mathbf{k} - \mathbf{p}), \tag{1}$$

$$\langle \Lambda_{c,1/2}^*(\mathbf{k}', r') | \Lambda_{c,1/2}^*(\mathbf{p}', s') \rangle = \delta_{r's'} 2E_{\Lambda_{c,1/2}^*} (2\pi)^3 \delta^3(\mathbf{k}' - \mathbf{p}'), \tag{2}$$

$$\langle \Lambda_{c,3/2}^*(\mathbf{k}', r') | \Lambda_{c,3/2}^*(\mathbf{p}', s') \rangle = \delta_{r's'} 2E_{\Lambda_{c,3/2}^*} (2\pi)^3 \delta^3(\mathbf{k}' - \mathbf{p}'), \tag{3}$$

and work with Dirac and Rarita-Schwinger spinors satisfying

$$\sum_s u(m_{\Lambda_b}, \mathbf{p}, s) \bar{u}(m_{\Lambda_b}, \mathbf{p}, s) = m_{\Lambda_b} + \not{p}, \tag{4}$$

$$\sum_{s'} u(m_{\Lambda_{c,1/2}^*}, \mathbf{p}', s') \bar{u}(m_{\Lambda_{c,1/2}^*}, \mathbf{p}', s') = m_{\Lambda_{c,1/2}^*} + \not{p}', \tag{5}$$

$$\sum_{s'} u_\mu(m_{\Lambda_{c,3/2}^*}, \mathbf{p}', s') \bar{u}_\nu(m_{\Lambda_{c,3/2}^*}, \mathbf{p}', s') = -(m_{\Lambda_{c,3/2}^*} + \not{p}') \left(g_{\mu\nu} - \frac{1}{3}\gamma_\mu\gamma_\nu - \frac{2}{3m^2_{\Lambda_{c,3/2}^*}} p'_\mu p'_\nu - \frac{1}{3m_{\Lambda_{c,3/2}^*}} (\gamma_\mu p'_\nu - \gamma_\nu p'_\mu) \right). \tag{6}$$

In the equations throughout this paper, Minkowski-space gamma matrices and the metric $(g_{\mu\nu}) = \mathrm{diag}(1, -1, -1, -1)$ are used, except where indicated otherwise. We introduce the notation

$$\langle \Lambda_{c,1/2}^*(\mathbf{p}', s') | \bar{c} \Gamma b | \Lambda_b(\mathbf{p}, s) \rangle = \bar{u}(m_{\Lambda_{c,1/2}^*}, \mathbf{p}', s') \gamma_5 \mathcal{G}^{(\frac{1}{2}^-)}[\Gamma] u(m_{\Lambda_b}, \mathbf{p}, s), \tag{7}$$

$$\langle \Lambda^*_{c,3/2}(\mathbf{p}', s')|\bar{c}\Gamma b|\Lambda_b(\mathbf{p}, s)\rangle = \bar{u}_\lambda(m_{\Lambda^*_{c,3/2}}, \mathbf{p}', s')\mathcal{G}^{\lambda(\frac{3}{2}^-)}[\Gamma]u(m_{\Lambda_b}, \mathbf{p}, s), \tag{8}$$

and

$$s_\pm = (m_{\Lambda_b} \pm m_{\Lambda^*_c})^2 - q^2, \tag{9}$$

where $q = p - p'$. We use a helicity basis for all form factors. For the $J^P = \frac{1}{2}^-$ final state, our definition follows the one introduced previously for $J^P = \frac{1}{2}^+$ final states [39] except for the changes resulting from the opposite parity [note the γ_5 in Eq. (7)]:

$$\begin{aligned}\mathcal{G}^{(\frac{1}{2}^-)}[\gamma^\mu] = {} & f_0^{(\frac{1}{2}^-)}(m_{\Lambda_b} + m_{\Lambda^*_{c,1/2}})\frac{q^\mu}{q^2} \\ & + f_+^{(\frac{1}{2}^-)}\frac{m_{\Lambda_b} - m_{\Lambda^*_{c,1/2}}}{s_-}\left(p^\mu + p'^\mu - (m^2_{\Lambda_b} - m^2_{\Lambda^*_{c,1/2}})\frac{q^\mu}{q^2}\right) \quad + f_\perp^{(\frac{1}{2}^-)}\left(\gamma^\mu + \frac{2m_{\Lambda^*_{c,1/2}}}{s_-}p^\mu - \frac{2m_{\Lambda_b}}{s_-}p'^\mu\right),\end{aligned} \tag{10}$$

$$\begin{aligned}\mathcal{G}^{(\frac{1}{2}^-)}[\gamma^\mu\gamma_5] = {} & -g_0^{(\frac{1}{2}^-)}\gamma_5(m_{\Lambda_b} - m_{\Lambda^*_{c,1/2}})\frac{q^\mu}{q^2} - g_+^{(\frac{1}{2}^-)}\gamma_5\frac{m_{\Lambda_b} + m_{\Lambda^*_{c,1/2}}}{s_+}\left(p^\mu + p'^\mu - (m^2_{\Lambda_b} - m^2_{\Lambda^*_{c,1/2}})\frac{q^\mu}{q^2}\right) \\ & - g_\perp^{(\frac{1}{2}^-)}\gamma_5\left(\gamma^\mu - \frac{2m_{\Lambda^*_{c,1/2}}}{s_+}p^\mu - \frac{2m_{\Lambda_b}}{s_+}p'^\mu\right),\end{aligned} \tag{11}$$

$$\mathcal{G}^{(\frac{1}{2}^-)}[i\sigma^{\mu\nu}q_\nu] = -h_+^{(\frac{1}{2}^-)}\frac{q^2}{s_-}\left(p^\mu + p'^\mu - (m^2_{\Lambda_b} - m^2_{\Lambda^*_{c,1/2}})\frac{q^\mu}{q^2}\right) - h_\perp^{(\frac{1}{2}^-)}(m_{\Lambda_b} - m_{\Lambda^*_{c,1/2}})\left(\gamma^\mu + \frac{2m_{\Lambda^*_{c,1/2}}}{s_-}p^\mu - \frac{2m_{\Lambda_b}}{s_-}p'^\mu\right), \tag{12}$$

$$\mathcal{G}^{(\frac{1}{2}^-)}[i\sigma^{\mu\nu}\gamma_5 q_\nu] = -\tilde{h}_+^{(\frac{1}{2}^-)}\gamma_5\frac{q^2}{s_+}\left(p^\mu + p'^\mu - (m^2_{\Lambda_b} - m^2_{\Lambda^*_{c,1/2}})\frac{q^\mu}{q^2}\right) - \tilde{h}_\perp^{(\frac{1}{2}^-)}\gamma_5(m_{\Lambda_b} + m_{\Lambda^*_{c,1/2}})\left(\gamma^\mu - \frac{2m_{\Lambda^*_{c,1/2}}}{s_+}p^\mu - \frac{2m_{\Lambda_b}}{s_+}p'^\mu\right). \tag{13}$$

For the $J^P = \frac{3}{2}^-$ final state, we use the definition introduced by us in Ref. [38], which reads

$$\begin{aligned}\mathcal{G}^{\lambda(\frac{3}{2}^-)}[\gamma^\mu] = {} & f_0^{(\frac{3}{2}^-)}\frac{m_{\Lambda^*_{c,3/2}}}{s_+}\frac{(m_{\Lambda_b} - m_{\Lambda^*_{c,3/2}})p^\lambda q^\mu}{q^2} \\ & + f_+^{(\frac{3}{2}^-)}\frac{m_{\Lambda^*_{c,3/2}}}{s_-}\frac{(m_{\Lambda_b} + m_{\Lambda^*_{c,3/2}})p^\lambda(q^2(p^\mu + p'^\mu) - (m^2_{\Lambda_b} - m^2_{\Lambda^*_{c,3/2}})q^\mu)}{q^2 s_+} \\ & + f_\perp^{(\frac{3}{2}^-)}\frac{m_{\Lambda^*_{c,3/2}}}{s_-}\left(p^\lambda\gamma^\mu - \frac{2p^\lambda(m_{\Lambda_b}p'^\mu + m_{\Lambda^*_{c,3/2}}p^\mu)}{s_+}\right) \\ & + f_{\perp'}^{(\frac{3}{2}^-)}\frac{m_{\Lambda^*_{c,3/2}}}{s_-}\left(p^\lambda\gamma^\mu - \frac{2p^\lambda p'^\mu}{m_{\Lambda^*_{c,3/2}}} + \frac{2p^\lambda(m_{\Lambda_b}p'^\mu + m_{\Lambda^*_{c,3/2}}p^\mu)}{s_+} + \frac{s_- g^{\lambda\mu}}{m_{\Lambda^*_{c,3/2}}}\right),\end{aligned} \tag{14}$$

$$\begin{aligned}\mathcal{G}^{\lambda(\frac{3}{2}^-)}[\gamma^\mu\gamma_5] = {} & -g_0^{(\frac{3}{2}^-)}\gamma_5\frac{m_{\Lambda^*_{c,3/2}}}{s_-}\frac{(m_{\Lambda_b} + m_{\Lambda^*_{c,3/2}})p^\lambda q^\mu}{q^2} \\ & - g_+^{(\frac{3}{2}^-)}\gamma_5\frac{m_{\Lambda^*_{c,3/2}}}{s_+}\frac{(m_{\Lambda_b} - m_{\Lambda^*_{c,3/2}})p^\lambda(q^2(p^\mu + p'^\mu) - (m^2_{\Lambda_b} - m^2_{\Lambda^*_{c,3/2}})q^\mu)}{q^2 s_-} \\ & - g_\perp^{(\frac{3}{2}^-)}\gamma_5\frac{m_{\Lambda^*_{c,3/2}}}{s_+}\left(p^\lambda\gamma^\mu - \frac{2p^\lambda(m_{\Lambda_b}p'^\mu - m_{\Lambda^*_{c,3/2}}p^\mu)}{s_-}\right) \\ & - g_{\perp'}^{(\frac{3}{2}^-)}\gamma_5\frac{m_{\Lambda^*_{c,3/2}}}{s_+}\left(p^\lambda\gamma^\mu + \frac{2p^\lambda p'^\mu}{m_{\Lambda^*_{c,3/2}}} + \frac{2p^\lambda(m_{\Lambda_b}p'^\mu - m_{\Lambda^*_{c,3/2}}p^\mu)}{s_-} - \frac{s_+ g^{\lambda\mu}}{m_{\Lambda^*_{c,3/2}}}\right),\end{aligned} \tag{15}$$

$$\mathcal{G}^{\lambda(\frac{3}{2}^-)}[i\sigma^{\mu\nu}q_\nu] = -h_+^{(\frac{3}{2}^-)}\frac{m_{\Lambda^*_{c,3/2}}}{s_-}\frac{p^\lambda(q^2(p^\mu+p'^\mu)-(m^2_{\Lambda_b}-m^2_{\Lambda^*_{c,3/2}})q^\mu)}{s_+}$$
$$- h_\perp^{(\frac{3}{2}^-)}\frac{m_{\Lambda^*_{c,3/2}}}{s_-}(m_{\Lambda_b}+m_{\Lambda^*_{c,3/2}})\left(p^\lambda\gamma^\mu-\frac{2p^\lambda(m_{\Lambda_b}p'^\mu+m_{\Lambda^*_{c,3/2}}p^\mu)}{s_+}\right)$$
$$- h_{\perp'}^{(\frac{3}{2}^-)}\frac{m_{\Lambda^*_{c,3/2}}}{s_-}(m_{\Lambda_b}+m_{\Lambda^*_{c,3/2}})\left(p^\lambda\gamma^\mu-\frac{2p^\lambda p'^\mu}{m_{\Lambda^*_{c,3/2}}}+\frac{2p^\lambda(m_{\Lambda_b}p'^\mu+m_{\Lambda^*_{c,3/2}}p^\mu)}{s_+}+\frac{s_-g^{\lambda\mu}}{m_{\Lambda^*_{c,3/2}}}\right), \quad (16)$$

$$\mathcal{G}^{\lambda(\frac{3}{2}^-)}[i\sigma^{\mu\nu}q_\nu\gamma_5] = -\tilde{h}_+^{(\frac{3}{2}^-)}\gamma_5\frac{m_{\Lambda^*_{c,3/2}}}{s_+}\frac{p^\lambda(q^2(p^\mu+p'^\mu)-(m^2_{\Lambda_b}-m^2_{\Lambda^*_{c,3/2}})q^\mu)}{s_-}$$
$$- \tilde{h}_\perp^{(\frac{3}{2}^-)}\gamma_5\frac{m_{\Lambda^*_{c,3/2}}}{s_+}(m_{\Lambda_b}-m_{\Lambda^*_{c,3/2}})\left(p^\lambda\gamma^\mu-\frac{2p^\lambda(m_{\Lambda_b}p'^\mu-m_{\Lambda^*_{c,3/2}}p^\mu)}{s_-}\right)$$
$$- \tilde{h}_{\perp'}^{(\frac{3}{2}^-)}\gamma_5\frac{m_{\Lambda^*_{c,3/2}}}{s_+}(m_{\Lambda_b}-m_{\Lambda^*_{c,3/2}})\left(p^\lambda\gamma^\mu+\frac{2p^\lambda p'^\mu}{m_{\Lambda^*_{c,3/2}}}+\frac{2p^\lambda(m_{\Lambda_b}p'^\mu-m_{\Lambda^*_{c,3/2}}p^\mu)}{s_-}-\frac{s_+g^{\lambda\mu}}{m_{\Lambda^*_{c,3/2}}}\right). \quad (17)$$

Only the vector and axial-vector form factors are needed to describe $\Lambda_b \to \Lambda_c^* \ell^- \bar{\nu}$ decays in the Standard Model, but we also compute the tensor form factors. Above, $\sigma^{\mu\nu} = \frac{i}{2}(\gamma^\mu\gamma^\nu - \gamma^\nu\gamma^\mu)$. Note that the overall sign of the form factors for each decay mode depends on the phase conventions of the states. This means that also the relative overall sign between the two different final states is left undetermined. Relations between our form-factor definitions and alternative definitions used in the literature are given in the Appendix.

III. LATTICE ACTIONS AND PARAMETERS

The lattice actions and parameters used in this work are the same as in our calculation of $\Lambda_b \to \Lambda^*(1520)$ form factors [38], except that here the valence strange quark is replaced by a valence charm quark. For the latter, we employ the same form of action and analogous tuning conditions as for the bottom quark [40], i.e., an anisotropic clover action with bare parameters $am_Q^{(c)}$, $\nu^{(c)}$, $c_{E,B}^{(c)}$ tuned to obtain the correct D_s meson kinetic mass, rest mass, and hyperfine splitting (our notation for the bare parameters follows Ref. [41], while Ref. [40] uses $m_0 = m_Q$, $\zeta = \nu$, $c_P = c_E = c_B$). The values of these parameters are given in Table I. The gauge-field ensembles with $2+1$ flavors of domain-wall fermions were generated by the RBC and UKQCD Collaborations [42,43]. For the up and down valence quarks, we reuse the domain-wall propagators computed for Ref. [38]. Our computation utilizes all-mode averaging [44,45], in which unbiased estimates with small statistical uncertainties are obtained at reduced cost by combining "exact" and "sloppy" samples.

IV. TWO-POINT FUNCTIONS AND HADRON MASSES

We now move to the discussion of the baryon interpolating fields, two-point functions, and results for the masses. For the Λ_b, everything is identical to Ref. [38]. The $\Lambda_c^*(2625)$ has the same isospin and spin-parity quantum numbers as the $\Lambda^*(1520)$ ($I = 0$, $J^P = \frac{3}{2}^-$), but with a charm quark instead of a strange quark. We therefore use the interpolating field

TABLE I. Parameters of the lattice actions, lattice spacings, and numbers of exact (ex) and sloppy (sl) samples computed for the correlation functions. The light-quark and gluon actions and the determination of the lattice spacings are described in Refs. [42,43]. The form of the heavy-quark action is given in Ref. [40], where $m_0 = m_Q$, $\zeta = \nu$, $c_P = c_E = c_B$.

Label	$N_s^3 \times N_t$	β	a [fm]	$am_{u,d}$	am_s	$am_Q^{(b)}$	$\nu^{(b)}$	$c_{E,B}^{(b)}$	$am_Q^{(c)}$	$\nu^{(c)}$	$c_{E,B}^{(c)}$	N_{ex}	N_{sl}
C01	$24^3 \times 64$	2.13	0.1106(3)	0.01	0.04	7.3258	3.1918	4.9625	0.1541	1.2004	1.8407	283	9056
C005	$24^3 \times 64$	2.13	0.1106(3)	0.005	0.04	7.3258	3.1918	4.9625	0.1541	1.2004	1.8407	311	9952
F004	$32^3 \times 64$	2.25	0.0828(3)	0.004	0.03	3.2823	2.0600	2.7960	−0.0517	1.1021	1.4483	251	8032

TABLE II. Paramters of the quark-field smearing used in the baryon interpolating fields. See Ref. [38] for explanations.

	Up and down quarks				Bottom quarks				Charm quarks			
	N_{Gauss}	σ_{Gauss}/a	N_{APE}	α_{APE}	N_{Gauss}	σ_{Gauss}/a	N_{Stout}	ρ_{Stout}	N_{Gauss}	σ_{Gauss}/a	N_{Stout}	ρ_{Stout}
Coarse	30	4.350	25	2.5	10	2.000	10	0.08	20	3.000	10	0.08
Fine	60	5.728	25	2.5	10	2.000	10	0.08	20	3.000	10	0.08

$$(O_{\Lambda_c^*})_{j\gamma} = \epsilon^{abc}(C\gamma_5)_{\alpha\beta}\left(\frac{1+\gamma_0}{2}\right)_{\gamma\delta} \times [\tilde{c}^a_\alpha \tilde{d}^b_\beta (\tilde{\nabla}_j \tilde{u})^c_\delta - \tilde{c}^a_\alpha \tilde{u}^b_\beta (\tilde{\nabla}_j \tilde{d})^c_\delta + \tilde{u}^a_\alpha (\tilde{\nabla}_j \tilde{d})^b_\beta \tilde{c}^c_\delta - \tilde{d}^a_\alpha (\tilde{\nabla}_j \tilde{u})^b_\beta \tilde{c}^c_\delta], \tag{18}$$

which differs from Eq. (18) of Ref. [38] only by the replacement $s \to c$. As before, this form will work only at zero momentum. The tilde indicates gauge-covariant Gaussian smearing of the quark fields with the parameters given in Table II. The field (18) actually has nonzero overlap with both the $\Lambda_c^*(2595)$ and the $\Lambda_c^*(2625)$,

$$\langle 0|(O_{\Lambda_c^*})_j|\Lambda^*_{c,1/2}(\mathbf{0}, s')\rangle = Z_{\Lambda^*_{c,1/2}} \frac{1+\gamma_0}{2}\gamma_j\gamma_5 u(m_{\Lambda^*_{c,1/2}}, \mathbf{0}, s'), \tag{19}$$

$$\langle 0|(O_{\Lambda_c^*})_j|\Lambda^*_{c,3/2}(\mathbf{0}, s')\rangle = Z_{\Lambda^*_{c,3/2}} \frac{1+\gamma_0}{2} u_j(m_{\Lambda^*_{c,3/2}}, \mathbf{0}, s'), \tag{20}$$

and we can isolate the $J = \frac{1}{2}$ and $J = \frac{3}{2}$ components[1] using the projectors

$$P^{kj}_{(1/2)} = \frac{1}{3}\gamma^k\gamma^j, \tag{21}$$

$$P^{kj}_{(3/2)} = g^{kj} - \frac{1}{3}\gamma^k\gamma^j. \tag{22}$$

The zero-momentum Λ_c^* two-point functions are defined like those for the Λ^* in Ref. [38], and after applying the above projectors their spectral decomposition reads

$$P^{jl}_{(1/2)} C^{(2,\Lambda_c^*)}_{lk}(t) = -\frac{1}{2} Z^2_{\Lambda^*_{c,1/2}}(1+\gamma_0)\gamma^j\gamma_k e^{-m_{\Lambda^*_{c,1/2}} t} + (\text{excited-state contributions}), \tag{23}$$

$$P^{jl}_{(3/2)} C^{(2,\Lambda_c^*)}_{lk}(t) = -\frac{1}{2} Z^2_{\Lambda^*_{c,3/2}}(1+\gamma_0)\left(g^j{}_k - \frac{1}{3}\gamma^j\gamma_k\right) e^{-m_{\Lambda^*_{c,3/2}} t} + (\text{excited-state contributions}). \tag{24}$$

At this point the reader may wonder why we did not analyze the $\Lambda^*(1405)$ with $J^P = \frac{1}{2}^-$ in Ref. [38], despite being able to project to $J^P = \frac{1}{2}^-$ with the available data. The reason is that we do not trust the single-hadron/narrow-width approximation for the $\Lambda^*(1405)$, which has a larger decay width than the $\Lambda^*(1520)$ and likely a two-pole structure [47].

The masses extracted from single-exponential fits to our results for $P^{jl}_{(1/2)}C^{(2,\Lambda_c^*)}$ and $P^{jl}_{(3/2)}C^{(2,\Lambda_c^*)}$ in the plateau regions are given in Table III, along with the masses of potential decay products. The latter are not used in our determination of the form factors but are included to assess whether the Λ_c^* baryons are stable under the strong interactions for our quark masses. We find that both $m_{\Lambda^*_{c,1/2}}$ and $m_{\Lambda^*_{c,3/2}}$ are lower than all of the following: $m_{\Lambda_c} + m_\pi + m_\pi$, $m_{\Sigma_c} + m_\pi$, $m_D + m_N$, although the difference $m_{\Lambda^*_{c,3/2}} - m_{\Sigma_c} - m_\pi$ becomes consistent with zero for the F004 ensemble within the statistical uncertainties. The results are of course affected by the finite volume to some degree, but it appears likely that both the $\Lambda^*_{c,1/2}$ and the $\Lambda^*_{c,3/2}$ are stable hadrons at least on the C01 and C005 ensembles, where the energies are well below all thresholds.

We also performed simple chiral-continuum extrapolations of $m_{\Lambda^*_{c,1/2}}$ and $m_{\Lambda^*_{c,3/2}}$ of the form

$$m_{\Lambda^*_{c,J}} = m^{(\text{phys})}_{\Lambda^*_{c,J}}\left[1 + c_J \frac{m_\pi^2 - m^2_{\pi,\text{phys}}}{(4\pi f_\pi)^2} + d_J a^2\Lambda^2\right] \tag{25}$$

with fit parameters $m^{(\text{phys})}_{\Lambda^*_{c,J}}$, c_J, d_J, and constants $f_\pi = 132$ MeV, $\Lambda = 300$ MeV. These fits yield $m^{(\text{phys})}_{\Lambda^*_{c,1/2}} = 2693(43)$ MeV, $m^{(\text{phys})}_{\Lambda^*_{c,3/2}} = 2742(43)$ MeV. To estimate systematic uncertainties associated with the choice of fit model, we additionally performed higher-order fits of the form

[1]At zero momentum, the continuum $J^P = \frac{1}{2}^-$ and $J^P = \frac{3}{2}^-$ irreducible representations subduce identically to the G_1^u and H^u irreducible representations of the double cover of the cubic group [46]; the next-higher values of J^P that subduce to the same cubic irreps are $\frac{7}{2}^-$ and $J^P = \frac{5}{2}^-$, respectively, and such states will have higher energies. It is therefore safe to refer to only the continuum quantum numbers in this case.

TABLE III. Hadron masses in GeV. We did not compute Σ_c two-point functions in this work and the Σ_c masses were estimated by adding the $\Sigma_c - \Lambda_c$ mass differences computed in Ref. [41] on the same ensembles with a slightly different tuning of the charm-quark action to the Λ_c masses computed here.

Label	m_π	m_D	m_N	m_{Λ_c}	$m_{\Sigma_c}^{(\mathrm{est})}$	$m_{\Lambda_{c,1/2}^*}$	$m_{\Lambda_{c,3/2}^*}$	$m_{\Lambda_{c,3/2}^*} - m_{\Lambda_{c,1/2}^*}$	m_{Λ_b}
C01	0.4312(13)	1.9119(54)	1.2647(51)	2.4652(82)	2.617(10)	2.882(12)	2.909(12)	0.0265(85)	5.793(17)
C005	0.3400(11)	1.8942(54)	1.1649(58)	2.4038(75)	2.565(12)	2.819(13)	2.839(13)	0.0185(97)	5.726(17)
F004	0.3030(12)	1.8880(70)	1.1197(59)	2.367(12)	2.550(19)	2.781(18)	2.815(18)	0.033(17)	5.722(23)

$$m_{\Lambda_{c,J}^*} = m_{\Lambda_{c,J}^*,\mathrm{HO}}^{(\mathrm{phys})}\left[1 + c_{J,\mathrm{HO}}\frac{m_\pi^2 - m_{\pi,\mathrm{phys}}^2}{(4\pi f_\pi)^2} + h_{J,\mathrm{HO}}\frac{m_\pi^3 - m_{\pi,\mathrm{phys}}^3}{(4\pi f_\pi)^3} + d_{J,\mathrm{HO}}a^2\Lambda^2 + g_{J,\mathrm{HO}}a^3\Lambda^3\right], \tag{26}$$

with Gaussian priors $h_{J,\mathrm{HO}} = 0 \pm 10$ and $g_{J,\mathrm{HO}} = 0 \pm 10$, and computed the systematic uncertainties using

$$\sigma_{m,\mathrm{syst}} = \max\left(|m_{\mathrm{HO}} - m|, \sqrt{|\sigma_{m,\mathrm{HO}}^2 - \sigma_m^2|}\right), \tag{27}$$

where m, σ_m denote the central value and uncertainty obtained using the parameter values and covariance matrix of the nominal fit and m_{HO}, $\sigma_{m,\mathrm{HO}}^2$ denote the central value and uncertainty obtained using the parameter values and covariance matrix of the higher-order fit. In this way we finally obtain

$$m_{\Lambda_{c,1/2}^*}^{(\mathrm{phys})} = (2693 \pm 43_{\mathrm{stat}} \pm 95_{\mathrm{syst}})\ \mathrm{MeV}, \tag{28}$$

$$m_{\Lambda_{c,3/2}^*}^{(\mathrm{phys})} = (2742 \pm 43_{\mathrm{stat}} \pm 96_{\mathrm{syst}})\ \mathrm{MeV}, \tag{29}$$

which are consistent with the experimental values of $m_{\Lambda_{c,1/2}^*} = 2592.25(28)$ MeV, $m_{\Lambda_{c,3/2}^*} = 2628.11(19)$ MeV [23]. Plots of the extrapolations are shown in Fig. 1. Note that we do not use the chiral-continuum extrapolations of the baryon masses in our determination of the form factors; we use the lattice baryon masses when computing the form factors on each ensemble, and then extrapolate only the form factors themselves. The mass extrapolations merely provide a test of our methodology. Finally, in Table III we also list the hyperfine splittings $m_{\Lambda_{c,3/2}^*} - m_{\Lambda_{c,1/2}^*}$ computed on each ensemble. Their relative uncertainties are too large to obtain a useful chiral-continuum extrapolation, but the results are consistent within $<2\sigma$ with the experimental value of 35.86(34) MeV on each ensemble.

V. THREE-POINT FUNCTIONS AND FORM FACTORS

As in Ref. [38], we compute forward and backward three-point functions

$$C_{j\gamma\delta}^{(3,\mathrm{fw})}(\mathbf{p},\Gamma,t,t') = \sum_{\mathbf{y},\mathbf{z}} e^{-i\mathbf{p}\cdot(\mathbf{y}-\mathbf{z})}\langle (O_{\Lambda_c^*})_{j\gamma}(x_0,\mathbf{x}) \times J_\Gamma(x_0 - t + t', \mathbf{y})(\overline{O_{\Lambda_b}})_\delta(x_0 - t, \mathbf{z})\rangle, \tag{30}$$

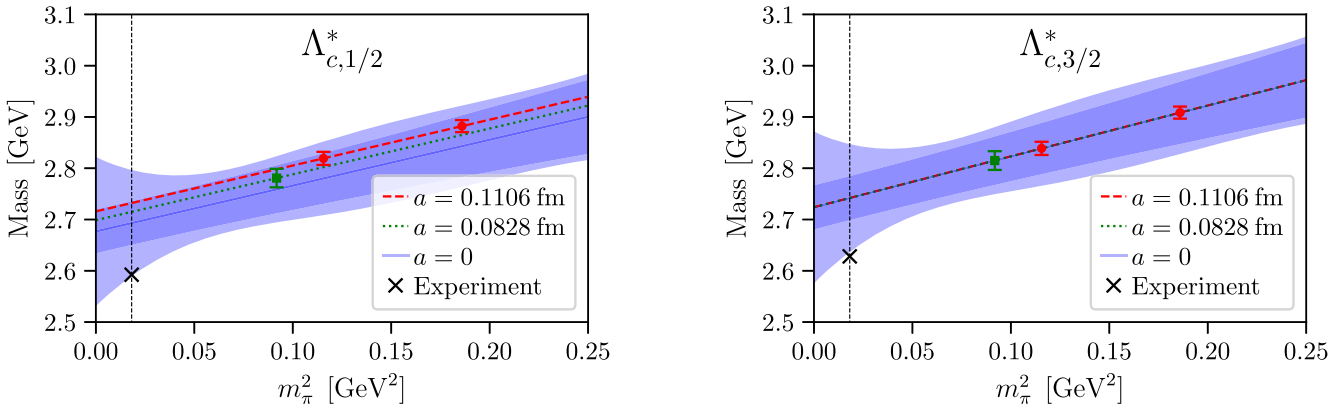

FIG. 1. Chiral and continuum extrapolations of our results for the $\Lambda_{c,1/2}^*$ and $\Lambda_{c,3/2}^*$ masses. The inner error bands are statistical only and the outer bands include estimates of the systematic uncertainties associated with these extrapolations. The experimental values from Ref. [23] are also shown.

TABLE IV. The values of the nonperturbative matching factors $Z_V^{(bb)}$ and $Z_V^{(cc)}$, determined using charge-conservation from ratios of zero-momentum B_s and D_s two-point and three-point functions, as well as the values of the $\mathcal{O}(a)$-improvement coefficients, computed at tree level in mean-field-improved perturbation theory.

	$Z_V^{(bb)}$	$Z_V^{(cc)}$	$d_1^{(b)}$	$d_1^{(c)}$
Coarse lattice (C01, C005)	9.0631(84)	1.35761(16)	0.0728	0.0412
Fine lattice (F004)	4.7449(21)	1.160978(74)	0.0696	0.0301

$$C^{(3,\mathrm{bw})}_{j\delta\gamma}(\mathbf{p},\Gamma,t,t-t') = \sum_{\mathbf{y},\mathbf{z}} e^{-i\mathbf{p}\cdot(\mathbf{z}-\mathbf{y})}\langle (O_{\Lambda_b})_\delta(x_0+t,\mathbf{z}) \times J^\dagger_\Gamma(x_0+t',\mathbf{y})(\overline{O_{\Lambda_c^*}})_{j\gamma}(x_0,\mathbf{x})\rangle, \tag{31}$$

where $\mathbf{p}$ is the Λ_b momentum, Γ is the Dirac matrix in the $b \to c$ weak current, t is the source-sink separation, and t' is the current-insertion time. With both the b and c quarks implemented using anisotropic clover actions, the current now includes $\mathcal{O}(a)$-improvement terms for both quarks:

$$J_\Gamma = \rho_\Gamma \sqrt{Z_V^{(cc)} Z_V^{(bb)}}[\bar{c}\Gamma b + a d_1^{(b)} \bar{c}\Gamma \boldsymbol{\gamma}_\mathrm{E}\cdot\overrightarrow{\boldsymbol{\nabla}} b - a d_1^{(c)} \bar{c}\overleftarrow{\boldsymbol{\nabla}}\cdot\boldsymbol{\gamma}_\mathrm{E}\Gamma b]. \tag{32}$$

Here, $\boldsymbol{\gamma}_\mathrm{E} = (\gamma^j_\mathrm{E}) = (-i\gamma^j)$ are the Euclidean spatial gamma matrices, and $\vec{\boldsymbol{\nabla}}$ are the gauge-covariant symmetric lattice derivatives. The overall matching factors in the current are written as $\rho_\Gamma\sqrt{Z_V^{(cc)}Z_V^{(bb)}}$ [48,49], where $Z_V^{(QQ)}$ are the matching factors for the flavor-conserving temporal vector currents $\bar{Q}\gamma^0 Q$. We determined the values of $Z_V^{(QQ)}$ nonperturbatively using the charge-conservation condition for three-point functions with D_s and B_s meson interpolating fields; the results are given in Table IV. With this choice, the residual matching factors ρ_Γ are equal to 1 at tree level and can be computed in perturbation theory without introducing large uncertainties. For the vector and axial-vector currents, we use the one-loop results given in Table III of Ref. [5]. Here we use more accurately tuned parameters in the b- and c-quark actions, but we expect the resulting change in the matching factors to be negligible. For the tensor currents, one-loop results are not presently available so we set $\rho_{\sigma_{\mu\nu}} = 1$ and estimate the resulting systematic uncertainty at $\mu = m_b$ to be 4.04% as in Ref. [10]. The values of the $\mathcal{O}(a)$-improvement coefficients for all currents are also computed at tree level and are given in Table IV.

We generated data for the same two choices of Λ_b momenta as in Ref. [38], $\mathbf{p} = (0,0,2)\frac{2\pi}{L}$ and $\mathbf{p} = (0,0,3)\frac{2\pi}{L}$, and for slightly larger source-sink separations: $t/a = 6\ldots14$ at the coarse lattice spacing and $t/a = 8\ldots16$ at the fine lattice spacing. Here we project the Λ_c^* field in the three-point functions to both $J = \frac{1}{2}$ and $J = \frac{3}{2}$, and the spectral decompositions read

$$P^{jl}_{(1/2)} C^{(3,\mathrm{fw})}_l(\mathbf{p},\Gamma,t,t') = \frac{1}{v^0} Z_{\Lambda^*_{c,1/2}} \frac{1+\gamma_0}{2}\gamma^j \mathcal{G}^{(\frac{1}{2}^-)}[\Gamma]\frac{1+\not{v}}{2}(Z^{(1)}_{\Lambda_b} + Z^{(2)}_{\Lambda_b}\gamma^0) e^{-m_{\Lambda^*_{c,1/2}}(t-t')} e^{-E_{\Lambda_b}t'} + (\text{excited-state contributions}), \tag{33}$$

$$P^{jl}_{(3/2)} C^{(3,\mathrm{fw})}_l(\mathbf{p},\Gamma,t,t') = -\frac{1}{v^0} Z_{\Lambda^*_{c,3/2}} \frac{1+\gamma_0}{2}\left(g^j{}_\lambda - \frac{1}{3}\gamma^j\gamma_\lambda - \frac{1}{3}\gamma^j g_{0\lambda}\right)\mathcal{G}^{\lambda(\frac{3}{2}^-)}[\Gamma]\frac{1+\not{v}}{2}(Z^{(1)}_{\Lambda_b} + Z^{(2)}_{\Lambda_b}\gamma^0) e^{-m_{\Lambda^*_{c,3/2}}(t-t')} e^{-E_{\Lambda_b}t'} + (\text{excited-state contributions}), \tag{34}$$

where $v^\mu = p^\mu/m_{\Lambda_b}$, and $\mathcal{G}^{(\frac{1}{2}^-)}[\Gamma]$, $\mathcal{G}^{\lambda(\frac{3}{2}^-)}[\Gamma]$ contain the form factors as explained in Sec. II.

In the following, we introduce a label $X \in \{V, A, TV, TA\}$ denoting the type of weak current, such that the matrix Γ in Eq. (32) is equal to

$$\Gamma^\mu_X = \begin{cases} \gamma^\mu & \text{for } X = V, \\ \gamma^\mu\gamma_5 & \text{for } X = A, \\ i\sigma^{\mu\nu}q_\nu & \text{for } X = TV, \\ i\sigma^{\mu\nu}q_\nu\gamma_5 & \text{for } X = TA. \end{cases} \tag{35}$$

We also introduce a label $\lambda \in \{0, +, \perp, \perp'\}$ for the different helicities. As in Ref. [38], we compute the quantities

$$F_\lambda^{(J^P)X}(\mathbf{p}, t) = \frac{S_\lambda^{(J^P)X}(\mathbf{p}, t, t/2)}{S_{\lambda_{\rm ref}}^{(J^P)X_{\rm ref}}(\mathbf{p}, t, t/2)} \sqrt{R_{\lambda_{\rm ref}}^{(J^P)X_{\rm ref}}(\mathbf{p})}, \tag{36}$$

where $J^P \in \{\frac{1}{2}^-, \frac{3}{2}^-\}$ are the quantum numbers of the Λ_c^*. Here, $R_{\lambda_{\rm ref}}^{(J^P)X_{\rm ref}}(\mathbf{p})$ denotes a constant fit at large t to a ratio $R_{\lambda_{\rm ref}}^{(J^P)X_{\rm ref}}(\mathbf{p}, t)$ of three-point and two-point functions that is constructed such that at large t it becomes equal to the square of the form factor associated with current $X_{\rm ref}$ and helicity $\lambda_{\rm ref}$. The quantities $S_\lambda^{(J^P)X}(\mathbf{p}, t, t/2)$ are linear projections of the three-point functions proportional to the form factor with current X and helicity λ. In this way, the relative signs of the form factors are preserved, and $F_\lambda^{(J^P)X}(\mathbf{p}, t)$ becomes equal to the form factor of interest at large t, which is then extracted from a constant fit. The choice of reference form factor $(X_{\rm ref}, \lambda_{\rm ref})$ is arbitrary in principle, and we select it based on the signal-to-noise ratio and quality of the ground-state plateau.

The equations for $J^P = \frac{3}{2}^-$ were given in Ref. [38] and we do not repeat them here. For $J^P = \frac{1}{2}^-$, the construction of $R_\lambda^{(\frac{1}{2}^-)X}(\mathbf{p}, t)$ is similar to that used previously for $J^P = \frac{1}{2}^+$ in Refs. [5,50]. We define

$$\mathcal{R}_0^{(\frac{1}{2}^-)X}(\mathbf{p}, t, t') = \frac{q_\mu q_\nu \mathrm{Tr}[\gamma_l P_{(1/2)}^{li} C_i^{(3,\mathrm{fw})}(\mathbf{p}, \Gamma_X^\mu, t, t')(1+\not{v}) C_n^{(3,\mathrm{bw})}(\mathbf{p}, \Gamma_X^\nu, t, t-t') P_{(1/2)}^{nm} \gamma_m]}{\mathrm{Tr}[P_{(1/2)}^{jk} C_{kj}^{(2,\Lambda_c^*)}(t)] \mathrm{Tr}[(1+\not{v}) C^{(2,\Lambda_b)}(\mathbf{p}, t)]}, \tag{37}$$

$$\mathcal{R}_+^{(\frac{1}{2}^-)X}(\mathbf{p}, t, t') = r_\mu[(1,\mathbf{0})] r_\nu[(1,\mathbf{0})] \frac{\mathrm{Tr}[\gamma_l P_{(1/2)}^{li} C_i^{(3,\mathrm{fw})}(\mathbf{p}, \Gamma_X^\mu, t, t')(1+\not{v}) C_n^{(3,\mathrm{bw})}(\mathbf{p}, \Gamma_X^\nu, t, t-t') P_{(1/2)}^{nm} \gamma_m]}{\mathrm{Tr}[P_{(1/2)}^{jk} C_{kj}^{(2,\Lambda_c^*)}(t)] \mathrm{Tr}[(1+\not{v}) C^{(2,\Lambda_b)}(\mathbf{p}, t)]}, \tag{38}$$

$$\mathcal{R}_\perp^{(\frac{1}{2}^-)X}(\mathbf{p}, t, t') = r_\mu[(0, \mathbf{e}_j \times \mathbf{p})] r_\nu[(0, \mathbf{e}_k \times \mathbf{p})] \frac{\mathrm{Tr}[\gamma_l P_{(1/2)}^{li} C_i^{(3,\mathrm{fw})}(\mathbf{p}, \Gamma_X^\mu, t, t') \gamma_5 \gamma^j (1+\not{v}) C_n^{(3,\mathrm{bw})}(\mathbf{p}, \Gamma_X^\nu, t, t-t') P_{(1/2)}^{nm} \gamma_m \gamma_5 \gamma^k]}{\mathrm{Tr}[P_{(1/2)}^{jk} C_{kj}^{(2,\Lambda_c^*)}(t)] \mathrm{Tr}[(1+\not{v}) C^{(2,\Lambda_b)}(\mathbf{p}, t)]}, \tag{39}$$

where

$$r[n] = n - \frac{(q \cdot n)}{q^2} q \tag{40}$$

for any four-vector n, and $\mathbf{e}_j$ denotes the three-dimensional unit vector in direction j. Above, repeated Greek indices are summed over from 0 to 3, while Latin indices are summed only over the spatial directions. The ratios $\mathcal{R}_\lambda^{(\frac{1}{2}^-)X}(\mathbf{p}, t, t')$ are equal to kinematic factors depending on the baryon energies times the squares of individual helicity form factors, up to excited-state contamination that decays exponentially for t and $t - t'$ both large. We then set $t' = t/2$ [or average over $(t+a)/2$ and $(t-a)/2$ in the case of odd t/a] and divide out the kinematic factors to obtain

$$\begin{aligned} R_0^{(\frac{1}{2}^-)V}(\mathbf{p}, t) &= \frac{4E_{\Lambda_b}}{3(m_{\Lambda_b} + m_{\Lambda_{c,1/2}^*})^2 (E_{\Lambda_b} - m_{\Lambda_b})} \mathcal{R}_0^{(\frac{1}{2}^-)V}(\mathbf{p}, t, t/2) \\ &= [f_0^{(\frac{1}{2}^-)}]^2 + (\text{excited-state contributions}), \end{aligned} \tag{41}$$

$$\begin{aligned} R_+^{(\frac{1}{2}^-)V}(\mathbf{p}, t) &= \frac{4E_{\Lambda_b} q^4}{3(E_{\Lambda_b} + m_{\Lambda_b})^2 (E_{\Lambda_b} - m_{\Lambda_b})(m_{\Lambda_b} - m_{\Lambda_{c,1/2}^*})^2} \mathcal{R}_+^{(\frac{1}{2}^-)V}(\mathbf{p}, t, t/2) \\ &= [f_+^{(\frac{1}{2}^-)}]^2 + (\text{excited-state contributions}), \end{aligned} \tag{42}$$

$$\begin{aligned} R_\perp^{(\frac{1}{2}^-)V}(\mathbf{p}, t) &= \frac{E_{\Lambda_b}}{3(E_{\Lambda_b} + m_{\Lambda_b})^2 (E_{\Lambda_b} - m_{\Lambda_b})} \mathcal{R}_\perp^{(\frac{1}{2}^-)V}(\mathbf{p}, t, t/2) \\ &= [f_\perp^{(\frac{1}{2}^-)}]^2 + (\text{excited-state contributions}), \end{aligned} \tag{43}$$

$$R_0^{(\frac{1}{2}^-)A}(\mathbf{p},t) = \frac{4E_{\Lambda_b}}{3(m_{\Lambda_b} - m_{\Lambda^*_{c,1/2}})^2(E_{\Lambda_b} + m_{\Lambda_b})}\mathcal{R}_0^{(\frac{1}{2}^-)A}(\mathbf{p},t,t/2)$$
$$= [g_0^{(\frac{1}{2}^-)}]^2 + (\text{excited-state contributions}), \tag{44}$$

$$R_+^{(\frac{1}{2}^-)A}(\mathbf{p},t) = \frac{4E_{\Lambda_b}q^4}{3(E_{\Lambda_b} - m_{\Lambda_b})^2(E_{\Lambda_b} + m_{\Lambda_b})(m_{\Lambda_b} + m_{\Lambda^*_{c,1/2}})^2}\mathcal{R}_+^{(\frac{1}{2}^-)A}(\mathbf{p},t,t/2)$$
$$= [g_+^{(\frac{1}{2}^-)}]^2 + (\text{excited-state contributions}), \tag{45}$$

$$R_\perp^{(\frac{1}{2}^-)A}(\mathbf{p},t) = -\frac{E_{\Lambda_b}}{3(E_{\Lambda_b} - m_{\Lambda_b})^2(E_{\Lambda_b} + m_{\Lambda_b})}\mathcal{R}_\perp^{(\frac{1}{2}^-)A}(\mathbf{p},t,t/2)$$
$$= [g_\perp^{(\frac{1}{2}^-)}]^2 + (\text{excited-state contributions}), \tag{46}$$

$$R_+^{(\frac{1}{2}^-)TV}(\mathbf{p},t) = \frac{4E_{\Lambda_b}}{3(E_{\Lambda_b} + m_{\Lambda_b})^2(E_{\Lambda_b} - m_{\Lambda_b})}\mathcal{R}_+^{(\frac{1}{2}^-)TV}(\mathbf{p},t,t/2)$$
$$= [h_+^{(\frac{1}{2}^-)}]^2 + (\text{excited-state contributions}), \tag{47}$$

$$R_\perp^{(\frac{1}{2}^-)TV}(\mathbf{p},t) = \frac{E_{\Lambda_b}}{3(E_{\Lambda_b} + m_{\Lambda_b})^2(E_{\Lambda_b} - m_{\Lambda_b})(m_{\Lambda_b} - m_{\Lambda^*_{c,1/2}})^2}\mathcal{R}_\perp^{(\frac{1}{2}^-)TV}(\mathbf{p},t,t/2)$$
$$= [h_\perp^{(\frac{1}{2}^-)}]^2 + (\text{excited-state contributions}), \tag{48}$$

$$R_+^{(\frac{1}{2}^-)TA}(\mathbf{p},t) = \frac{4E_{\Lambda_b}}{3(E_{\Lambda_b} - m_{\Lambda_b})^2(E_{\Lambda_b} + m_{\Lambda_b})}\mathcal{R}_+^{(\frac{1}{2}^-)TA}(\mathbf{p},t,t/2)$$
$$= [\tilde{h}_+^{(\frac{1}{2}^-)}]^2 + (\text{excited-state contributions}), \tag{49}$$

$$R_\perp^{(\frac{1}{2}^-)TA}(\mathbf{p},t) = -\frac{E_{\Lambda_b}}{3(E_{\Lambda_b} - m_{\Lambda_b})^2(E_{\Lambda_b} + m_{\Lambda_b})(m_{\Lambda_b} + m_{\Lambda^*_{c,1/2}})^2}\mathcal{R}_\perp^{(\frac{1}{2}^-)TA}(\mathbf{p},t,t/2)$$
$$= [\tilde{h}_\perp^{(\frac{1}{2}^-)}]^2 + (\text{excited-state contributions}). \tag{50}$$

The linear projections of the three-point functions are constructed using

$$\mathcal{S}_\lambda^{(\frac{1}{2}^-)V,TV}(\mathbf{p},t,t') = \mathrm{Tr}\left[M_{\mu j}^{(\lambda)}P_{(1/2)}^{jl}C_l^{(3,\mathrm{fw})}(\mathbf{p},\Gamma_{V,TV}^\mu,t,t')\frac{(1+\not{v})}{2}\right], \tag{51}$$

$$\mathcal{S}_\lambda^{(\frac{1}{2}^-)A,TA}(\mathbf{p},t,t') = \mathrm{Tr}\left[\gamma_5 M_{\mu j}^{(\lambda)}P_{(1/2)}^{jl}C_l^{(3,\mathrm{fw})}(\mathbf{p},\Gamma_{A,TA}^\mu,t,t')\frac{(1+\not{v})}{2}\right], \tag{52}$$

where

$$M_{\mu j}^{(0)} = \epsilon_\mu^{(0)}\epsilon_j^{(0)}, \tag{53}$$

$$M_{\mu j}^{(+)} = \epsilon_\mu^{(+)}\epsilon_j^{(0)}, \tag{54}$$

$$M_{\mu j}^{(\perp)} = \sum_{i=1}^{3}\epsilon_\mu^{(\perp,i)}\epsilon_j^{(\perp,i)}, \tag{55}$$

with the polarization vectors

$$\epsilon^{(0)} = (q^0, \mathbf{q}), \qquad \epsilon^{(+)} = (|\mathbf{q}|, (q^0/|\mathbf{q}|)\mathbf{q}), \qquad \epsilon^{(\perp,j)} = (0, \mathbf{e}_j \times \mathbf{q}). \tag{56}$$

To improve the signals, we use the average of the forward three-point function and the Dirac adjoint of the backward three-point function instead of just $C^{(3,\mathrm{fw})}$. We then divide out appropriate kinematic factors to obtain

$$\begin{aligned} S_0^{(\frac{1}{2}^-)V}(\mathbf{p},t,t') &= -\frac{E_{\Lambda_b} m_{\Lambda_b}}{(E_{\Lambda_b} - m_{\Lambda_b})(E_{\Lambda_b} + m_{\Lambda_b})(m_{\Lambda_b} + m_{\Lambda^*_{c,1/2}})} \mathcal{S}_0^{(\frac{1}{2}^-)V}(\mathbf{p},t,t') \\ &= f_0^{(\frac{1}{2}^-)} Z_{\Lambda^*_{c,1/2}} (Z^{(1)}_{\Lambda_b} m_{\Lambda_b} + Z^{(2)}_{\Lambda_b} E_{\Lambda_b}) e^{-m_{\Lambda^*_{c,1/2}}(t-t')} e^{-E_{\Lambda_b} t'} + (\text{excited-state contributions}), \end{aligned} \tag{57}$$

$$\begin{aligned} S_+^{(\frac{1}{2}^-)V}(\mathbf{p},t,t') &= -\frac{E_{\Lambda_b} m_{\Lambda_b}}{(E_{\Lambda_b} - m_{\Lambda_b})^{1/2}(E_{\Lambda_b} + m_{\Lambda_b})^{3/2}(m_{\Lambda_b} - m_{\Lambda^*_{c,1/2}})} \mathcal{S}_+^{(\frac{1}{2}^-)V}(\mathbf{p},t,t') \\ &= f_+^{(\frac{1}{2}^-)} Z_{\Lambda^*_{c,1/2}} (Z^{(1)}_{\Lambda_b} m_{\Lambda_b} + Z^{(2)}_{\Lambda_b} E_{\Lambda_b}) e^{-m_{\Lambda^*_{c,1/2}}(t-t')} e^{-E_{\Lambda_b} t'} + (\text{excited-state contributions}), \end{aligned} \tag{58}$$

$$\begin{aligned} S_\perp^{(\frac{1}{2}^-)V}(\mathbf{p},t,t') &= -\frac{E_{\Lambda_b} m_{\Lambda_b}}{2(E_{\Lambda_b} - m_{\Lambda_b})(E_{\Lambda_b} + m_{\Lambda_b})^2} \mathcal{S}_\perp^{(\frac{1}{2}^-)V}(\mathbf{p},t,t') \\ &= f_\perp^{(\frac{1}{2}^-)} Z_{\Lambda^*_{c,1/2}} (Z^{(1)}_{\Lambda_b} m_{\Lambda_b} + Z^{(2)}_{\Lambda_b} E_{\Lambda_b}) e^{-m_{\Lambda^*_{c,1/2}}(t-t')} e^{-E_{\Lambda_b} t'} + (\text{excited-state contributions}), \end{aligned} \tag{59}$$

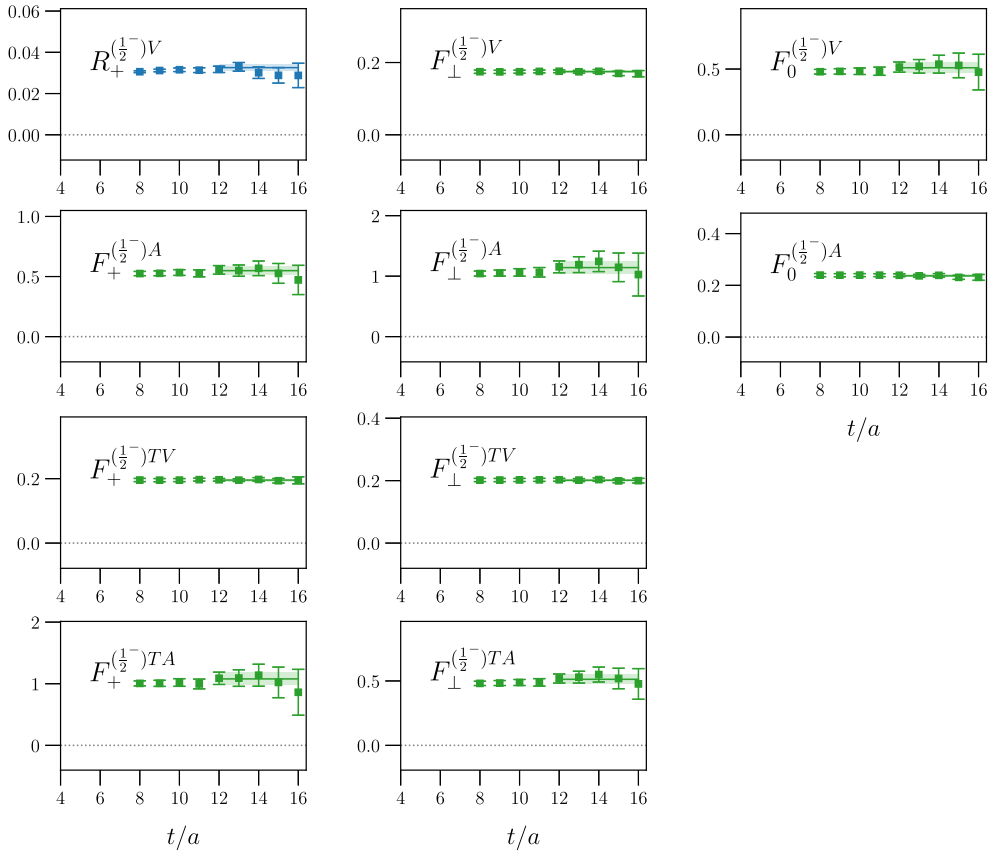

FIG. 2. Numerical results for the quantities $F_\lambda^{(\frac{1}{2}^-)X}(\mathbf{p},t)$, defined in Eq. (36), as a function of the source-sink separation, for $\mathbf{p} = (0,0,2)\frac{2\pi}{L}$ and for the F004 ensemble. Also shown is $R_+^{(\frac{1}{2}^-)V}(\mathbf{p},t)$, which is used to extract the square of the reference form factor $f_+^{(\frac{1}{2}^-)}$. The horizontal lines indicate the ranges and extracted values of constant fits.

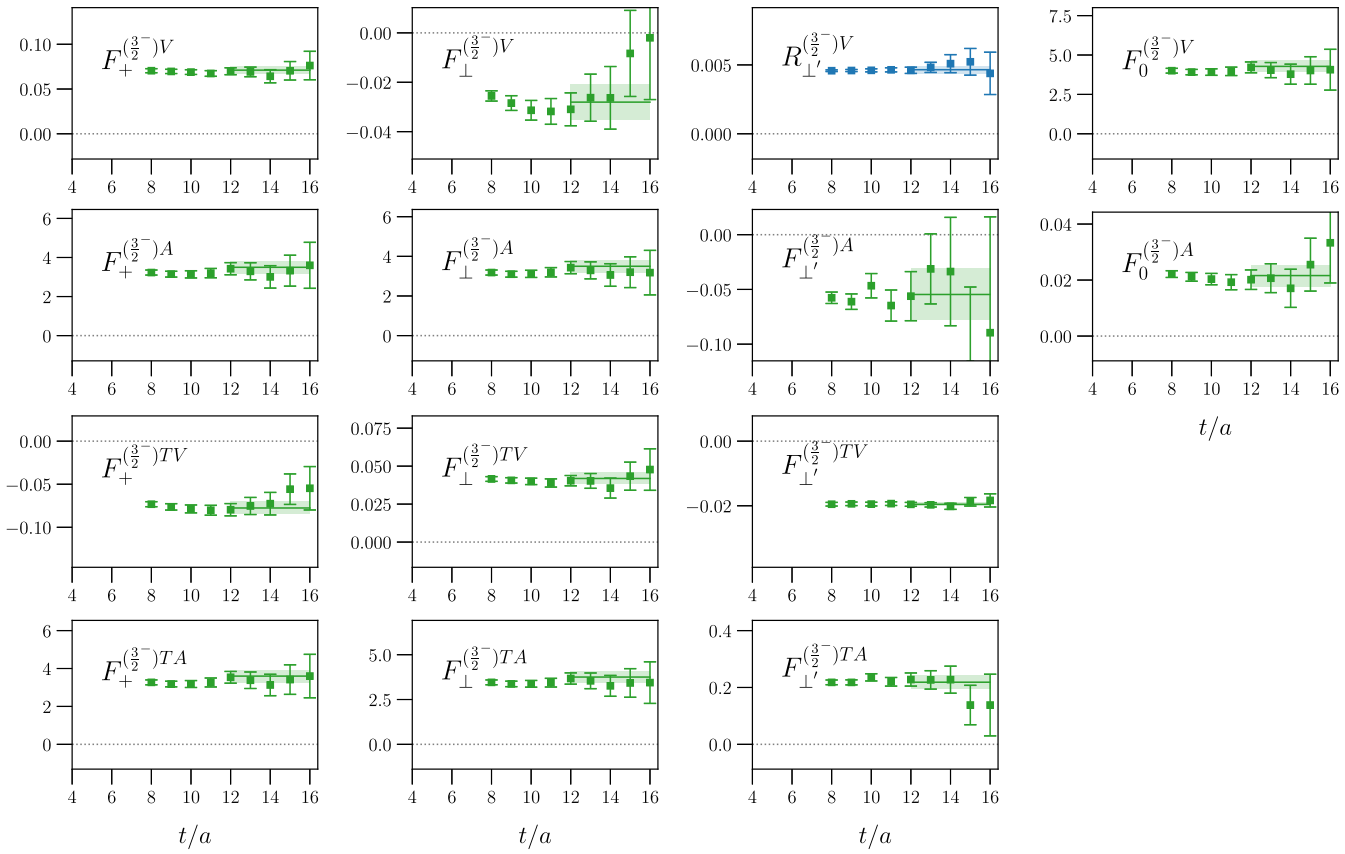

FIG. 3. Numerical results for the quantities $F_\lambda^{(\frac{3}{2}^-)X}(\mathbf{p}, t)$, defined in Eq. (36), as a function of the source-sink separation, for $\mathbf{p} = (0, 0, 2)\frac{2\pi}{L}$ and for the F004 ensemble. Also shown is $R_{\perp'}^{(\frac{3}{2}^-)V}(\mathbf{p}, t)$, which is used to extract the square of the reference form factor $f_{\perp'}^{(\frac{3}{2}^-)}$. The horizontal lines indicate the ranges and extracted values of constant fits.

$$S_0^{(\frac{1}{2}^-)A}(\mathbf{p}, t, t') = -\frac{E_{\Lambda_b} m_{\Lambda_b}}{(E_{\Lambda_b} - m_{\Lambda_b})(E_{\Lambda_b} + m_{\Lambda_b})(m_{\Lambda_b} - m_{\Lambda^*_{c,1/2}})} \mathcal{S}_0^{(\frac{1}{2}^-)A}(\mathbf{p}, t, t')$$
$$= g_0^{(\frac{1}{2}^-)} Z_{\Lambda^*_{c,1/2}} (Z^{(1)}_{\Lambda_b} m_{\Lambda_b} + Z^{(2)}_{\Lambda_b} E_{\Lambda_b}) e^{-m_{\Lambda^*_{c,1/2}}(t-t')} e^{-E_{\Lambda_b} t'} + (\text{excited-state contributions}), \quad (60)$$

$$S_+^{(\frac{1}{2}^-)A}(\mathbf{p}, t, t') = -\frac{E_{\Lambda_b} m_{\Lambda_b}}{(E_{\Lambda_b} - m_{\Lambda_b})^{3/2}(E_{\Lambda_b} + m_{\Lambda_b})^{1/2}(m_{\Lambda_b} + m_{\Lambda^*_{c,1/2}})} \mathcal{S}_+^{(\frac{1}{2}^-)A}(\mathbf{p}, t, t')$$
$$= g_+^{(\frac{1}{2}^-)} Z_{\Lambda^*_{c,1/2}} (Z^{(1)}_{\Lambda_b} m_{\Lambda_b} + Z^{(2)}_{\Lambda_b} E_{\Lambda_b}) e^{-m_{\Lambda^*_{c,1/2}}(t-t')} e^{-E_{\Lambda_b} t'} + (\text{excited-state contributions}), \quad (61)$$

$$S_\perp^{(\frac{1}{2}^-)A}(\mathbf{p}, t, t') = \frac{E_{\Lambda_b} m_{\Lambda_b}}{2(E_{\Lambda_b} - m_{\Lambda_b})^2(E_{\Lambda_b} + m_{\Lambda_b})} \mathcal{S}_\perp^{(\frac{1}{2}^-)A}(\mathbf{p}, t, t')$$
$$= g_\perp^{(\frac{1}{2}^-)} Z_{\Lambda^*_{c,1/2}} (Z^{(1)}_{\Lambda_b} m_{\Lambda_b} + Z^{(2)}_{\Lambda_b} E_{\Lambda_b}) e^{-m_{\Lambda^*_{c,1/2}}(t-t')} e^{-E_{\Lambda_b} t'} + (\text{excited-state contributions}), \quad (62)$$

$$S_+^{(\frac{1}{2}^-)TV}(\mathbf{p}, t, t') = \frac{E_{\Lambda_b} m_{\Lambda_b}}{(E_{\Lambda_b} - m_{\Lambda_b})^{1/2}(E_{\Lambda_b} + m_{\Lambda_b})^{3/2} q^2} \mathcal{S}_+^{(\frac{1}{2}^-)TV}(\mathbf{p}, t, t')$$
$$= h_+^{(\frac{1}{2}^-)} Z_{\Lambda^*_{c,1/2}} (Z^{(1)}_{\Lambda_b} m_{\Lambda_b} + Z^{(2)}_{\Lambda_b} E_{\Lambda_b}) e^{-m_{\Lambda^*_{c,1/2}}(t-t')} e^{-E_{\Lambda_b} t'} + (\text{excited-state contributions}), \quad (63)$$

$$S_{\perp}^{(\frac{1}{2}^-)TV}(\mathbf{p},t,t') = \frac{E_{\Lambda_b} m_{\Lambda_b}}{2(E_{\Lambda_b}-m_{\Lambda_b})(E_{\Lambda_b}+m_{\Lambda_b})^2(m_{\Lambda_b}-m_{\Lambda^*_{c,1/2}})} \mathcal{S}_{\perp}^{(\frac{1}{2}^-)TV}(\mathbf{p},t,t')$$
$$= h_{\perp}^{(\frac{1}{2}^-)} Z_{\Lambda^*_{c,1/2}} (Z^{(1)}_{\Lambda_b} m_{\Lambda_b} + Z^{(2)}_{\Lambda_b} E_{\Lambda_b}) e^{-m_{\Lambda^*_{c,1/2}}(t-t')} e^{-E_{\Lambda_b} t'} + (\text{excited-state contributions}), \quad (64)$$

$$S_{+}^{(\frac{1}{2}^-)TA}(\mathbf{p},t,t') = -\frac{E_{\Lambda_b} m_{\Lambda_b}}{(E_{\Lambda_b}+m_{\Lambda_b})^{1/2}(E_{\Lambda_b}-m_{\Lambda_b})^{3/2} q^2} \mathcal{S}_{+}^{(\frac{1}{2}^-)TA}(\mathbf{p},t,t')$$
$$= \tilde{h}_{+}^{(\frac{1}{2}^-)} Z_{\Lambda^*_{c,1/2}} (Z^{(1)}_{\Lambda_b} m_{\Lambda_b} + Z^{(2)}_{\Lambda_b} E_{\Lambda_b}) e^{-m_{\Lambda^*_{c,1/2}}(t-t')} e^{-E_{\Lambda_b} t'} + (\text{excited-state contributions}), \quad (65)$$

$$S_{\perp}^{(\frac{1}{2}^-)TA}(\mathbf{p},t,t') = \frac{E_{\Lambda_b} m_{\Lambda_b}}{2(E_{\Lambda_b}+m_{\Lambda_b})(E_{\Lambda_b}-m_{\Lambda_b})^2(m_{\Lambda_b}+m_{\Lambda^*_{c,1/2}})} \mathcal{S}_{\perp}^{(\frac{1}{2}^-)TA}(\mathbf{p},t,t')$$
$$= \tilde{h}_{\perp}^{(\frac{1}{2}^-)} Z_{\Lambda^*_{c,1/2}} (Z^{(1)}_{\Lambda_b} m_{\Lambda_b} + Z^{(2)}_{\Lambda_b} E_{\Lambda_b}) e^{-m_{\Lambda^*_{c,1/2}}(t-t')} e^{-E_{\Lambda_b} t'} + (\text{excited-state contributions}), \quad (66)$$

such that the unwanted factors of $Z_{\Lambda^*_{c,1/2}} (Z^{(1)}_{\Lambda_b} m_{\Lambda_b} + Z^{(2)}_{\Lambda_b} E_{\Lambda_b}) e^{-m_{\Lambda^*_{c,1/2}}(t-t')} e^{-E_{\Lambda_b} t'}$ cancel in Eq. (36) at large t.

For $J^P = \frac{1}{2}^-$, we use $X_{\text{ref}} = V$, $\lambda_{\text{ref}} = +$. Sample results for $F_{\lambda}^{(\frac{1}{2}^-)X}(\mathbf{p},t)$ and our constant fits thereof are shown in Fig. 2. For $J^P = \frac{3}{2}^-$, we use $X_{\text{ref}} = V$, $\lambda_{\text{ref}} = \perp'$ as in Ref. [38]. Sample results for $F_{\lambda}^{(\frac{3}{2}^-)X}(\mathbf{p},t)$ and our constant fits thereof are shown in Fig. 3. The values of the form factors obtained from the constant fits are listed in Tables V and VI. The fits were done individually for each form factor and take into account the correlations between the data at different t. The values of χ^2/d.o.f. range between approximately 0.5 and 1.0, where typically d.o.f. = 4. The correlations between the results for different form factors

TABLE V. Values of the $\Lambda_b \to \Lambda^*_{c,1/2}$ form factors for each ensemble and for the two different Λ_b momenta.

Form factor	$\lvert\mathbf{p}\rvert/(2\pi/L)$	C01	C005	F004
$f_0^{(\frac{1}{2}^-)}$	2	0.592(43)	0.550(54)	0.510(38)
	3	0.536(31)	0.496(38)	0.483(29)
$f_+^{(\frac{1}{2}^-)}$	2	0.1843(51)	0.1743(59)	0.1804(47)
	3	0.2005(68)	0.1887(80)	0.1990(65)
$f_\perp^{(\frac{1}{2}^-)}$	2	0.1728(39)	0.1692(47)	0.1748(37)
	3	0.1781(49)	0.1735(58)	0.1837(48)
$g_0^{(\frac{1}{2}^-)}$	2	0.2414(55)	0.2324(67)	0.2366(53)
	3	0.2521(73)	0.2433(88)	0.2511(71)
$g_+^{(\frac{1}{2}^-)}$	2	0.624(38)	0.601(49)	0.549(36)
	3	0.571(29)	0.542(35)	0.522(28)
$g_\perp^{(\frac{1}{2}^-)}$	2	1.35(11)	1.27(14)	1.14(10)
	3	1.205(80)	1.12(10)	1.063(72)
$h_+^{(\frac{1}{2}^-)}$	2	0.1935(42)	0.1896(52)	0.1956(40)
	3	0.1957(52)	0.1908(63)	0.2028(51)
$h_\perp^{(\frac{1}{2}^-)}$	2	0.2065(50)	0.1955(59)	0.2013(47)
	3	0.2203(67)	0.2081(79)	0.2172(64)
$\tilde{h}_+^{(\frac{1}{2}^-)}$	2	1.32(11)	1.24(14)	1.08(10)
	3	1.182(82)	1.09(10)	1.011(74)
$\tilde{h}_\perp^{(\frac{1}{2}^-)}$	2	0.576(39)	0.555(49)	0.513(36)
	3	0.528(29)	0.503(35)	0.486(27)

TABLE VI. Values of the $\Lambda_b \to \Lambda^*_{c,3/2}$ form factors for each ensemble and for the two different Λ_b momenta.

Form factor	$\lvert\mathbf{p}\rvert/(2\pi/L)$	C01	C005	F004
$f_0^{(\frac{3}{2}^-)}$	2	5.24(40)	4.68(47)	4.28(35)
	3	4.70(34)	4.05(35)	3.91(28)
$f_+^{(\frac{3}{2}^-)}$	2	0.0784(45)	0.0670(50)	0.0711(40)
	3	0.1074(72)	0.0904(76)	0.0949(60)
$f_\perp^{(\frac{3}{2}^-)}$	2	−0.0127(79)	−0.0295(90)	−0.0280(72)
	3	0.046(10)	0.020(11)	0.0205(88)
$f_{\perp'}^{(\frac{3}{2}^-)}$	2	0.0708(24)	0.0693(28)	0.0682(20)
	3	0.0658(32)	0.0634(37)	0.0639(27)
$g_0^{(\frac{3}{2}^-)}$	2	0.0305(41)	0.0194(48)	0.0216(38)
	3	0.0605(60)	0.0451(65)	0.0454(52)
$g_+^{(\frac{3}{2}^-)}$	2	4.41(36)	3.86(42)	3.50(32)
	3	3.94(30)	3.33(32)	3.16(25)
$g_\perp^{(\frac{3}{2}^-)}$	2	4.34(36)	3.86(42)	3.50(31)
	3	3.90(29)	3.36(31)	3.19(24)
$g_{\perp'}^{(\frac{3}{2}^-)}$	2	−0.037(29)	−0.048(31)	−0.055(24)
	3	−0.029(21)	−0.044(23)	−0.041(17)
$h_+^{(\frac{3}{2}^-)}$	2	−0.0609(81)	−0.0733(93)	−0.0776(74)
	3	−0.004(10)	−0.024(11)	−0.0296(87)
$h_\perp^{(\frac{3}{2}^-)}$	2	0.0490(40)	0.0379(46)	0.0419(36)
	3	0.0784(62)	0.0621(66)	0.0652(52)
$h_{\perp'}^{(\frac{3}{2}^-)}$	2	−0.01943(68)	−0.01839(75)	−0.01954(59)
	3	−0.0188(10)	−0.0172(10)	−0.01925(87)
$\tilde{h}_+^{(\frac{3}{2}^-)}$	2	4.43(36)	3.97(42)	3.60(32)
	3	3.98(30)	3.45(31)	3.27(25)
$\tilde{h}_\perp^{(\frac{3}{2}^-)}$	2	4.64(37)	4.06(43)	3.75(32)
	3	4.16(31)	3.52(32)	3.40(25)
$\tilde{h}_{\perp'}^{(\frac{3}{2}^-)}$	2	0.249(30)	0.223(31)	0.219(24)
	3	0.237(25)	0.198(24)	0.218(20)

and different momenta on a given ensemble were evaluated using bootstrap resampling.

VI. CHIRAL AND CONTINUUM EXTRAPOLATIONS OF THE FORM FACTORS

As in Ref. [38], we extrapolate the lattice results for the form factors to the continuum limit and the physical pion mass using the model

$$f(q^2) = F^f\left[1 + C^f\frac{m_\pi^2 - m_{\pi,\mathrm{phys}}^2}{(4\pi f_\pi)^2} + D^f a^2\Lambda^2\right] + A^f\left[1 + \tilde{C}^f\frac{m_\pi^2 - m_{\pi,\mathrm{phys}}^2}{(4\pi f_\pi)^2} + \tilde{D}^f a^2\Lambda^2\right](w-1) \tag{67}$$

with fit parameters F^f, A^f, C^f, D^f, $\tilde{C}^f$, $\tilde{D}^f$ for each form factor f, and using the kinematic variable

$$w(q^2) = v\cdot v' = \frac{m_{\Lambda_b}^2 + m_{\Lambda_c^*}^2 - q^2}{2m_{\Lambda_b}m_{\Lambda_c^*}}, \tag{68}$$

where $m_{\Lambda_c^*} = m_{\Lambda^*_{c,1/2}}$ or $m_{\Lambda_c^*} = m_{\Lambda^*_{c,3/2}}$ depending on the final state considered. In the physical limit $m_\pi = m_{\pi,\mathrm{phys}}$, $a = 0$, the functions reduce to

$$f(q^2) = F^f + A^f(w-1). \tag{69}$$

This parametrization corresponds to a Taylor expansion of the shape of the form factors around the end point $w = 1$, i.e., an expansion in powers of $(w-1)$; because we have lattice results for only two different kinematic points near $w = 1.01$ and $w = 1.03$, we work only to first order, and we expect the parametrization to become unreliable for large $(w-1)$. Our results for F^f and A^f from fits using Eq. (67) are given in the first two columns of Table VII, and the values and full covariance matrices (evaluated using bootstrap) are also provided as Supplemental Material [51]. As can be seen

in Figs. 4–7, the lattice data are well described by the model. The fits of the individual form factors have $\chi^2/\text{d.o.f.}$ in the range from approximately 0.5 to 1.5, where we count F^f, A^f, C^f, and D^f as parameters that are primarily constrained by the data, such that $\text{d.o.f.} = 6 - 4 = 2$.

Again following Ref. [38], to estimate systematic uncertainties associated with the chiral and continuum extrapolations, we also performed "higher-order" fits including additional terms describing the dependence on the lattice spacing and pion mass,

$$f_{\rm HO}(q^2) = F^f_{\rm HO}\left[1 + C^f_{\rm HO}\frac{m_\pi^2 - m_{\pi,\rm phys}^2}{(4\pi f_\pi)^2} + H^f_{\rm HO}\frac{m_\pi^3 - m_{\pi,\rm phys}^3}{(4\pi f_\pi)^3} + D^f_{\rm HO}a^2\Lambda^2 + E^f_{\rm HO}a\Lambda + G^f_{\rm HO}a^3\Lambda^3\right] + A^f_{\rm HO}\left[1 + \tilde{C}^f_{\rm HO}\frac{m_\pi^2 - m_{\pi,\rm phys}^2}{(4\pi f_\pi)^2} + \tilde{H}^f_{\rm HO}\frac{m_\pi^3 - m_{\pi,\rm phys}^3}{(4\pi f_\pi)^3} + \tilde{D}^f_{\rm HO}a^2\Lambda^2 + \tilde{E}^f_{\rm HO}a\Lambda + \tilde{G}^f_{\rm HO}a^3\Lambda^3\right](w-1). \quad (70)$$

No priors were used for the parameters F^f, A^f, $F^f_{\rm HO}$, $A^f_{\rm HO}$. The Gaussian priors for the parameters describing the lattice-spacing and pion-mass dependence were chosen as in Ref. [38] except for $E^f_{\rm HO}$ and $\tilde{E}^f_{\rm HO}$. These coefficients describe the effects of the incomplete $\mathcal{O}(a)$ improvement of the weak currents in Eq. (32), and here we take the prior widths for $E^f_{\rm HO}$ and $\tilde{E}^f_{\rm HO}$ to be two times larger than in Ref. [38], based on the observation in Ref. [5] that these effects may be larger for a heavy-to-heavy current than for a heavy-to-light current. These widths allow for missing $\mathcal{O}(a)$ corrections as large as 10% at the coarse lattice spacing, motivated by the large b-quark momenta used here. In the higher-order fits, we also multiplied the data for each form factor with Gaussian random distributions of central value 1 and appropriate widths to incorporate estimates of systematic uncertainties associated with the residual matching factors ρ_Γ (2% for the vector and axial vector currents, 4.04% for the tensor currents [10]) and systematic uncertainties associated with neglecting the down-up quark-mass difference and QED corrections [$\mathcal{O}((m_d - m_u)/\Lambda) \approx 0.8\%$ and $\mathcal{O}(\alpha_{\rm e.m.}) \approx 0.7\%$]. Furthermore, to include the scale-setting uncertainty, we also promoted the lattice spacings to fit parameters with Gaussian priors according to the values and uncertainties shown in Table I. All of our lattice calculations were performed with $m_\pi L > 4$, and we therefore expect finite-volume effects to be negligible at least for the heavier pion masses where the $\Lambda_c^*(2595)$ and $\Lambda_c^*(2625)$ are well below strong-decay thresholds. However, we are unable to provide a quantitative estimate of finite-volume effects in the extrapolated form factors.

In the physical limit, the higher-order fits reduce to the same form as in Eq. (69) but with parameters $F^f_{\rm HO}$ and $A^f_{\rm HO}$. Our results for these parameters are given in the last two columns in Table VII and also in Supplemental Material [51]. For any observable O, we evaluate the form-factor systematic uncertainty using

$$\sigma_{O,\rm syst} = \max\left(|O_{\rm HO} - O|, \sqrt{|\sigma^2_{O,\rm HO} - \sigma^2_O|}\right), \quad (71)$$

where O, σ_O denote the central value and uncertainty calculated using $\{F^f, A^f\}$ and their covariance matrix, and

TABLE VII. The parameters describing the $\Lambda_b \to \Lambda_c^*(2595)$ and $\Lambda_b \to \Lambda_c^*(2625)$ form factors at the physical pion mass and in the continuum limit. The nominal parameters F^f and A^f are used to evaluate the central values and statistical uncertainties, while the "higher-order" parameters $F^f_{\rm HO}$ and $A^f_{\rm HO}$ are used in combination with the nominal parameters to evaluate systematic uncertainties as explained in the main text. Files containing the parameter values and the covariance matrices are provided as Supplemental Material [51].

f	F^f	A^f	$F^f_{\rm HO}$	$A^f_{\rm HO}$
$f_0^{(\frac{1}{2}^-)}$	0.545(64)	−2.21(66)	0.546(75)	−2.20(69)
$f_+^{(\frac{1}{2}^-)}$	0.1628(90)	1.16(31)	0.164(14)	1.17(33)
$f_\perp^{(\frac{1}{2}^-)}$	0.1690(79)	0.57(25)	0.169(13)	0.58(26)
$g_0^{(\frac{1}{2}^-)}$	0.221(11)	0.94(33)	0.221(17)	0.95(35)
$g_+^{(\frac{1}{2}^-)}$	0.582(64)	−2.24(65)	0.584(76)	−2.23(68)
$g_\perp^{(\frac{1}{2}^-)}$	1.22(16)	−6.1(1.9)	1.22(18)	−6.1(2.0)
$h_+^{(\frac{1}{2}^-)}$	0.1908(89)	0.47(30)	0.191(14)	0.49(32)
$h_\perp^{(\frac{1}{2}^-)}$	0.1860(93)	0.98(28)	0.187(15)	0.98(30)
$\tilde{h}_+^{(\frac{1}{2}^-)}$	1.15(16)	−5.8(1.8)	1.15(18)	−5.7(1.9)
$\tilde{h}_\perp^{(\frac{1}{2}^-)}$	0.543(62)	−2.12(67)	0.544(75)	−2.11(71)
$f_0^{(\frac{3}{2}^-)}$	4.29(67)	−27.3(8.7)	4.31(75)	−27.0(8.8)
$f_+^{(\frac{3}{2}^-)}$	0.0498(70)	1.28(27)	0.0504(83)	1.29(29)
$f_\perp^{(\frac{3}{2}^-)}$	−0.073(14)	2.52(35)	−0.073(14)	2.54(39)
$f_{\perp'}^{(\frac{3}{2}^-)}$	0.0687(40)	−0.280(89)	0.0687(59)	−0.279(89)
$g_0^{(\frac{3}{2}^-)}$	0.0027(35)	1.23(21)	0.0027(36)	1.23(23)
$g_+^{(\frac{3}{2}^-)}$	3.46(58)	−24.7(8.1)	3.47(64)	−24.5(8.1)
$g_\perp^{(\frac{3}{2}^-)}$	3.47(57)	−22.6(7.8)	3.49(63)	−22.4(7.9)
$g_{\perp'}^{(\frac{3}{2}^-)}$	−0.062(38)	0.62(57)	−0.062(37)	0.62(57)
$h_+^{(\frac{3}{2}^-)}$	−0.124(16)	2.51(32)	−0.124(18)	2.52(37)
$h_\perp^{(\frac{3}{2}^-)}$	0.0208(53)	1.22(23)	0.0210(60)	1.22(25)
$h_{\perp'}^{(\frac{3}{2}^-)}$	−0.0201(12)	0.040(21)	−0.0201(19)	0.039(21)
$\tilde{h}_+^{(\frac{3}{2}^-)}$	3.58(59)	−23.7(8.1)	3.59(66)	−23.5(8.1)
$\tilde{h}_\perp^{(\frac{3}{2}^-)}$	3.72(61)	−25.1(8.2)	3.74(69)	−24.8(8.3)
$\tilde{h}_{\perp'}^{(\frac{3}{2}^-)}$	0.232(49)	−0.60(52)	0.235(56)	−0.60(56)

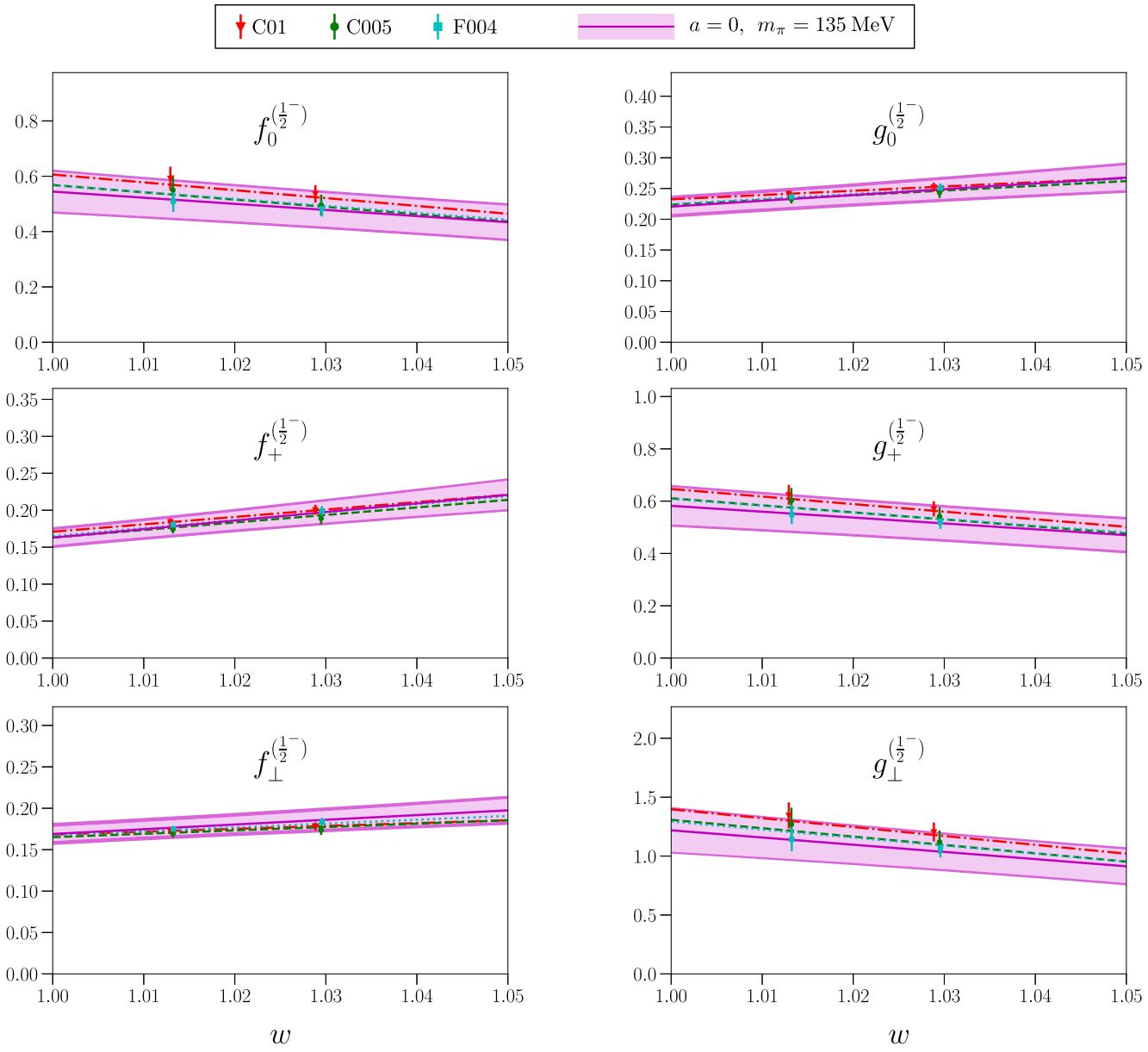

FIG. 4. Chiral and continuum extrapolations of the $\Lambda_b \to \Lambda_c^*(2595)$ vector and axial vector form factors. The solid magenta curves show the form factors in the physical limit $a = 0$, $m_\pi = 135$ MeV, with inner light magenta bands indicating the statistical uncertainties and outer dark magenta bands indicating the total uncertainties. The dashed-dotted, dashed, and dotted curves show the fit functions evaluated at the lattice spacings and pion masses of the individual data sets C01, C005, and F004, respectively, with uncertainty bands omitted for clarity.

$O_{\rm HO}$, $\sigma^2_{O,\rm HO}$ denote the central value and uncertainty calculated using $\{F^f_{\rm HO}, A^f_{\rm HO}\}$ and their covariance matrix. We find that the (vector and axial-vector) form-factor systematic uncertainties result in an approximately 12 to 13% systematic uncertainty in the $\Lambda_b \to \Lambda_c^*(2595)\mu^-\bar{\nu}$ differential decay rate in the kinematic range shown in Sec. VIII, and 14 to 18% for $\Lambda_b \to \Lambda_c^*(2625)\mu^-\bar{\nu}$. Because the decay rates depend quadratically on the form factors, this corresponds to "average" systematic uncertainties of around 6% in the $\Lambda_b \to \Lambda_c^*(2595)$ vector and axial-vector form factors and around 8% for $\Lambda_b \to \Lambda_c^*(2625)$.

VII. COMPARISON WITH ZERO-RECOIL SUM RULES

At zero recoil ($w = 1$), approximate sum-rule bounds on the size of heavy-to-heavy form factors can be derived using the operator product expansion and heavy-quark effective theory [24,25,52–55]. In Ref. [24], it was found that the lattice results for the $\Lambda_b \to \Lambda_c$ form factors with the $J^P = \frac{1}{2}^+$ final state (which constitute the "elastic" contribution to the sum rule) almost completely saturate the bounds derived through order $1/m^3$, apparently leaving very little room for "inelastic" contributions from other

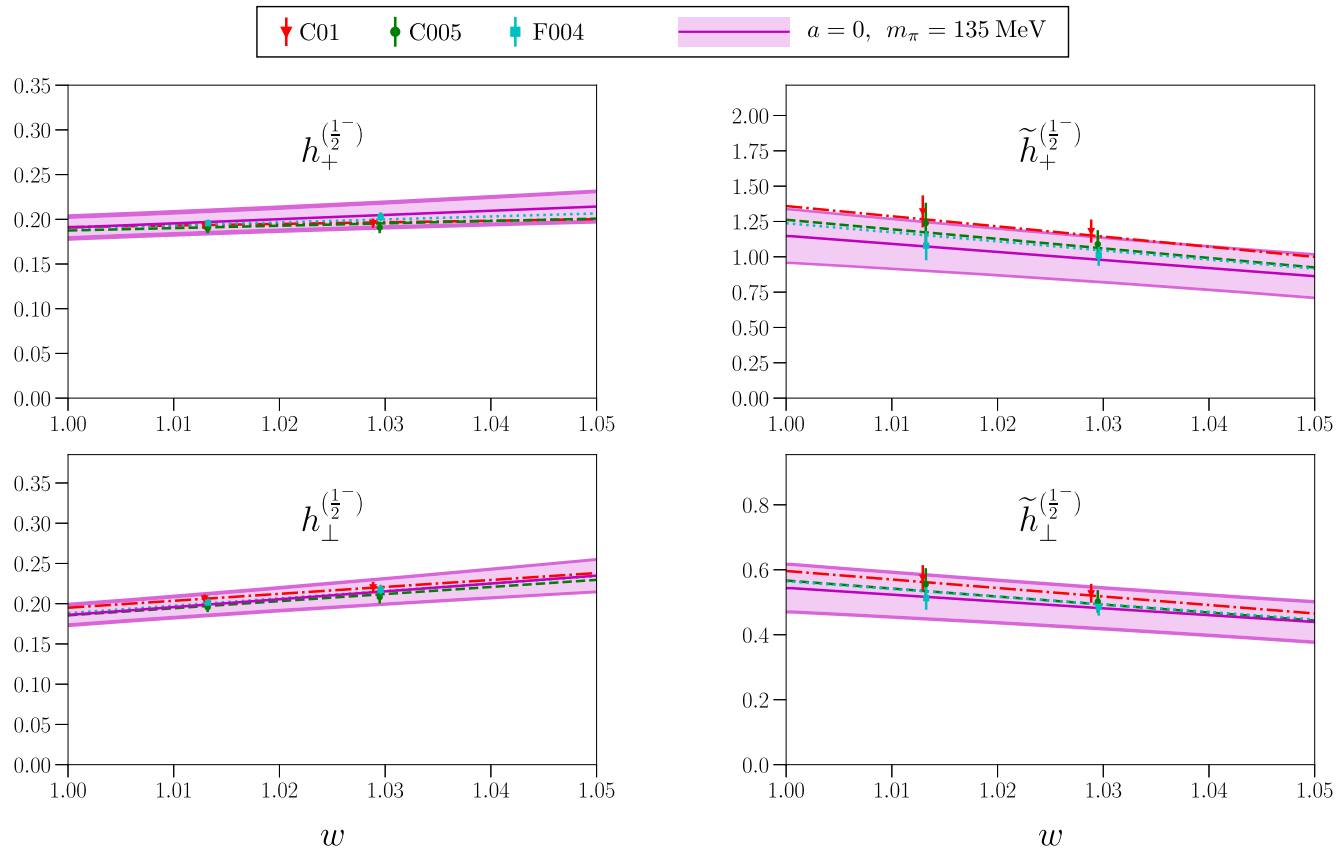

FIG. 5. Like Fig. 4, but for the $\Lambda_b \to \Lambda_c^*(2595)$ tensor form factors.

final states such as the Λ_c^*s considered here. However, in the case of B-meson decays, the size of $1/m^4$ and $1/m^5$ corrections has been found to be approximately 33% of the size of the $1/m^2$ and $1/m^3$ terms [25,55]. Allowing for effects of this size also for Λ_b decays, the authors of Ref. [25] then obtained estimates of the size of the inelastic contributions, which are expected to be dominated by $\Lambda_b \to \Lambda_c^*(2595)$ and $\Lambda_b \to \Lambda_c^*(2625)$.

When expressed in terms of our form-factor definitions using the relations given in Appendix A 3, Eqs. (46), (48), (50), and (52) of Ref. [25] become

$$F_{\mathrm{inel},1/2} = |f_+^{(\frac{1}{2}^-)}|^2_{w=1} + 2|f_\perp^{(\frac{1}{2}^-)}|^2_{w=1}, \tag{72}$$

$$F_{\mathrm{inel},3/2} = \frac{1}{6}\left[\frac{(m_{\Lambda_b} + m_{\Lambda_{c,3/2}^*})^2}{(m_{\Lambda_b} - m_{\Lambda_{c,3/2}^*})^2}|f_+^{(\frac{3}{2}^-)}|^2 + 2|f_\perp^{(\frac{3}{2}^-)}|^2 + 6|f_{\perp'}^{(\frac{3}{2}^-)}|^2\right]_{w=1}, \tag{73}$$

$$G_{\mathrm{inel},1/2} = \frac{1}{3}|g_0^{(\frac{1}{2}^-)}|^2_{w=1}, \tag{74}$$

$$G_{\mathrm{inel},3/2} = \frac{1}{18}\frac{(m_{\Lambda_b} + m_{\Lambda_{c,3/2}^*})^2}{(m_{\Lambda_b} - m_{\Lambda_{c,3/2}^*})^2}|g_0^{(\frac{3}{2}^-)}|^2_{w=1}. \tag{75}$$

The zero-recoil sum-rule estimate obtained in Ref. [25] is

$$F_{\mathrm{inel},1/2} + F_{\mathrm{inel},3/2} \approx 0.011^{+0.061}_{-0.055}, \tag{76}$$

$$G_{\mathrm{inel},1/2} + G_{\mathrm{inel},3/2} \approx 0.040^{+0.049}_{-0.052}. \tag{77}$$

Using our lattice-QCD results for the form factors, we find

$$F_{\mathrm{inel},1/2} + F_{\mathrm{inel},3/2} = 0.093 \pm 0.009_{\mathrm{stat}} \pm 0.012_{\mathrm{syst}}, \tag{78}$$

$$G_{\mathrm{inel},1/2} + G_{\mathrm{inel},3/2} = 0.0162 \pm 0.0016_{\mathrm{stat}} \pm 0.0020_{\mathrm{syst}}. \tag{79}$$

Thus, our result for the axial current falls within the range given in Ref. [25], while our result for the vector current is slightly above the upper limit.

VIII. $\Lambda_b \to \Lambda_c^* \ell^- \bar{\nu}$ OBSERVABLES

The two-fold differential decay rates of $\Lambda_b \to \Lambda_c^*(2595)\ell^-\bar{\nu}$ and $\Lambda_b \to \Lambda_c^*(2625)\ell^-\bar{\nu}$ in the Standard Model can be written as

$$\frac{\mathrm{d}^2\Gamma^{(J)}}{\mathrm{d}q^2\,\mathrm{d}\cos\theta_\ell} = A^{(J)} + B^{(J)}\cos\theta_\ell + C^{(J)}\cos^2\theta_\ell, \tag{80}$$

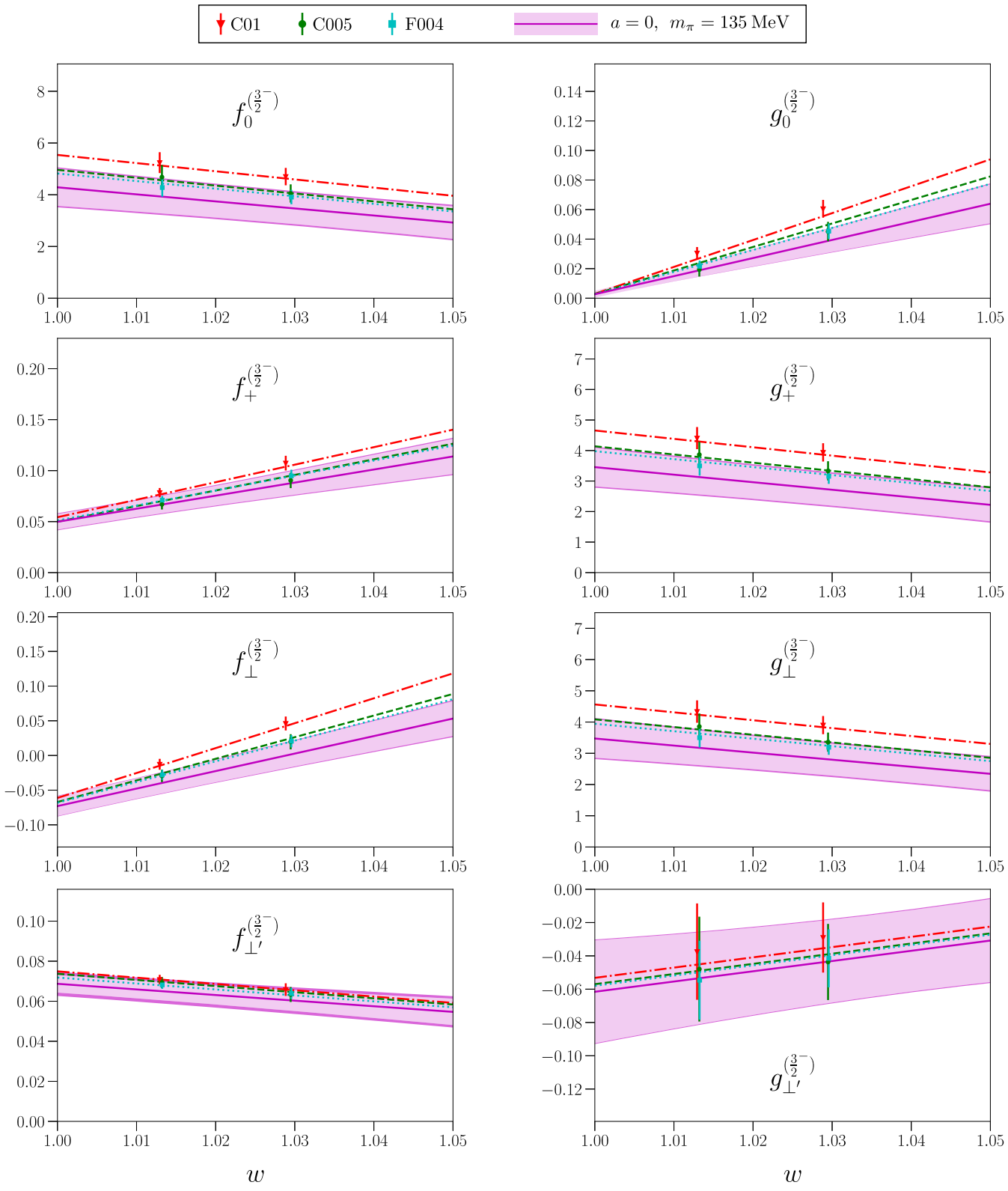

FIG. 6. Like Fig. 4, but for the $\Lambda_b \to \Lambda_c^*(2625)$ vector and axial vector form factors.

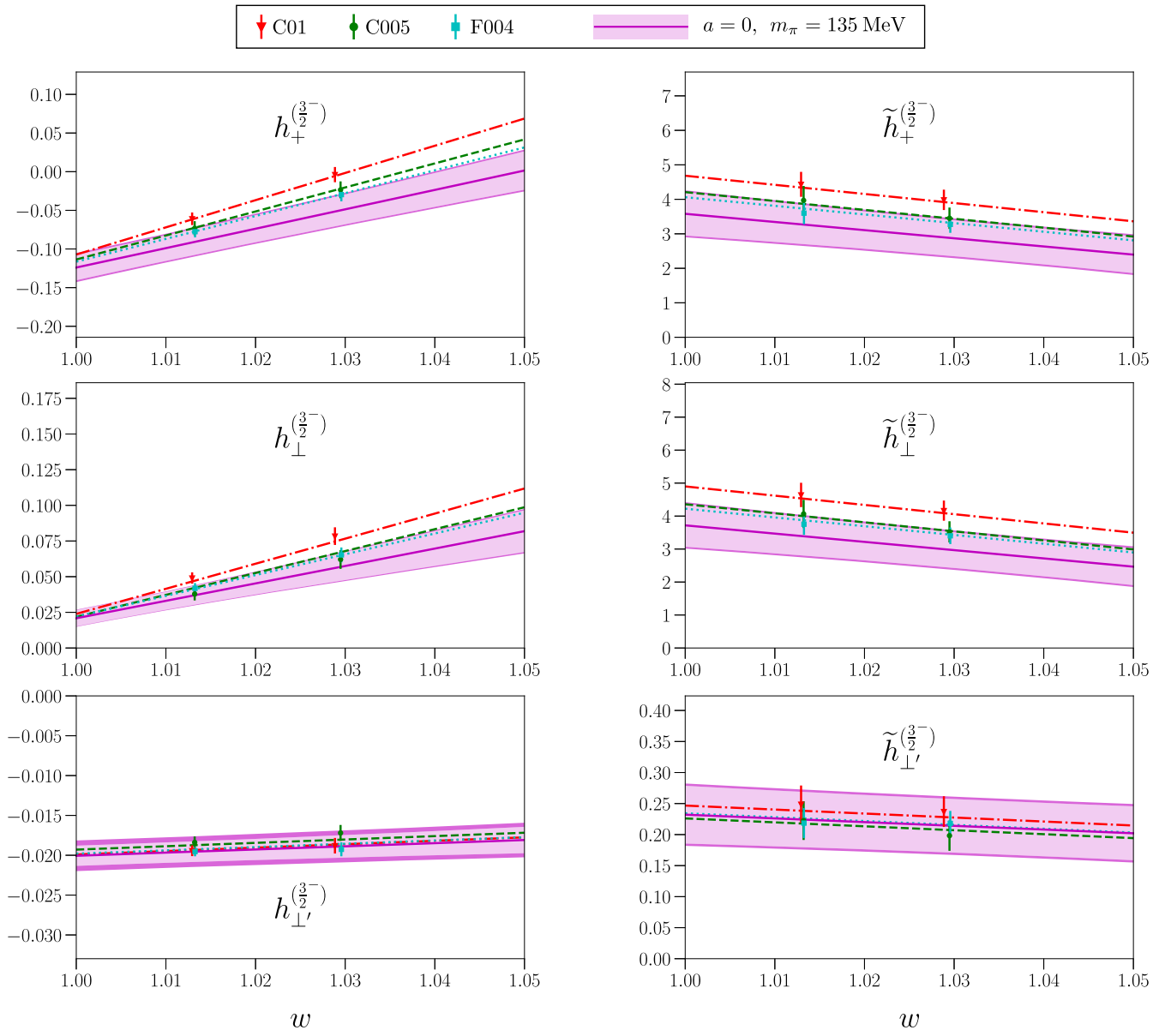

FIG. 7. Like Fig. 4, but for the $\Lambda_b \to \Lambda_c^*(2625)$ tensor form factors.

where θ_ℓ is the helicity angle of the charged lepton and $A^{(J)}$, $B^{(J)}$, $C^{(J)}$ are functions of q^2 only [25]. The $J = \frac{1}{2}, \frac{3}{2}$ superscript is used to distinguish the $\Lambda_c^*(2595)$ and $\Lambda_c^*(2625)$ final states. The equations for $A^{(J)}$, $B^{(J)}$, and $C^{(J)}$ in terms of the form factors are given in Ref. [25] (where $A^{(J)} = \Gamma_0^{(\ell)} a_\ell^{(J)}$ etc.) and can be converted to our conventions using the relations in Appendix A 3. The integral over $\cos\theta_\ell$ yields the q^2-differential decay rate

$$\frac{\mathrm{d}\Gamma^{(J)}}{\mathrm{d}q^2} = 2A^{(J)} + \frac{2}{3}C^{(J)}, \tag{81}$$

and we also consider two angular observables [25]: the forward-backward asymmetry

$$A_{FB}^{(J)} = \frac{B^{(J)}}{\mathrm{d}\Gamma^{(J)}/\mathrm{d}q^2} \tag{82}$$

and the "flat term"

$$F_H^{(J)} = \frac{2(A^{(J)} + C^{(J)})}{\mathrm{d}\Gamma^{(J)}/\mathrm{d}q^2}. \tag{83}$$

The Standard Model predictions for $\mathrm{d}\Gamma^{(J)}/\mathrm{d}q^2/|V_{cb}|^2$ and for the angular observables using our form-factor results are shown in Fig. 8. Note that at leading order in heavy-quark effective theory, the differential decay rate for the $J = \frac{1}{2}$ final state would be a factor of 2 smaller than the differential rate for $J = \frac{3}{2}$, and the lepton-side angular observables considered here would be equal for both final

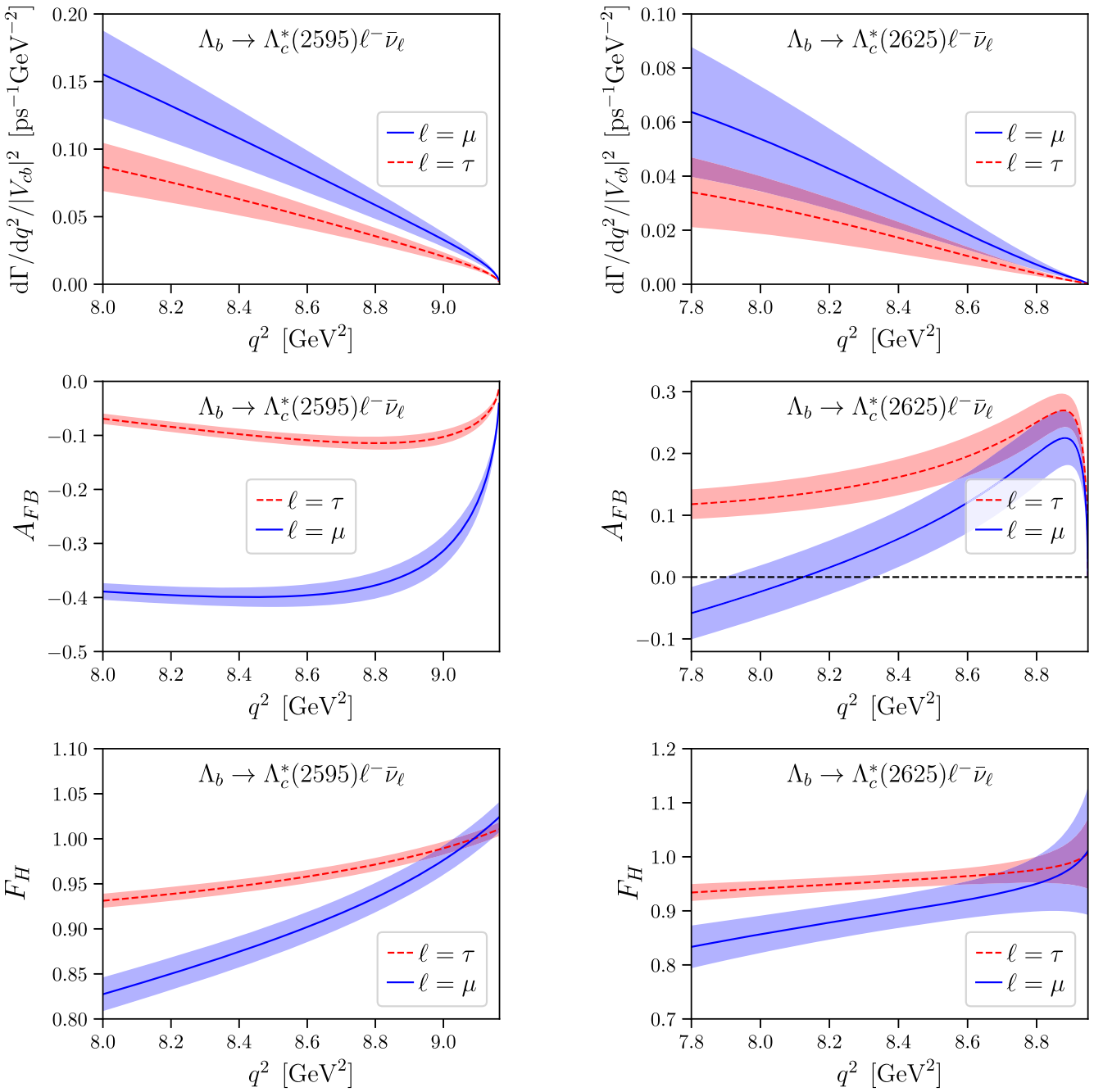

FIG. 8. $\Lambda_b \to \Lambda_c^*(2595)\ell^-\bar{\nu}$ (left) and $\Lambda_b \to \Lambda_c^*(2625)\ell^-\bar{\nu}$ (right) observables in the high-q^2 region calculated in the Standard Model using our form-factor results. From top to bottom: the differential decay rate divided by $|V_{cb}|^2$, the forward-backward asymmetry, and the flat term. In each case, we show results for $\ell = \mu$ and $\ell = \tau$ (the results for $\ell = e$ would look the same as for $\ell = \mu$ in this kinematic region). The bands indicate the total (statistical + systematic) uncertainties.

states [25,33]. In contrast, we find the $J = \frac{1}{2}$ rate to be approximately 2.5 times larger than the $J = \frac{3}{2}$ rate, and we find the forward-backward asymmetries to have opposite signs at high q^2. Leading-order HQET is of course expected to be inadequate for these decays, in which the light degrees of freedom in the final state have a different angular momentum than in the initial state. The forms of the subleading corrections are known [25,33], but we have not been able to obtain an acceptable HQET fit to the full set of form factors even when including these corrections, suggesting that sub-subleading terms may also be significant.

In Fig. 9 we additionally compare the $\Lambda_b \to \Lambda_c^*(2595)\mu^-\bar{\nu}$, and $\Lambda_b \to \Lambda_c^*(2625)\mu^-\bar{\nu}$ differential decay rates with that of $\Lambda_b \to \Lambda_c\mu^-\bar{\nu}$, using the form factors from Ref. [5] for the

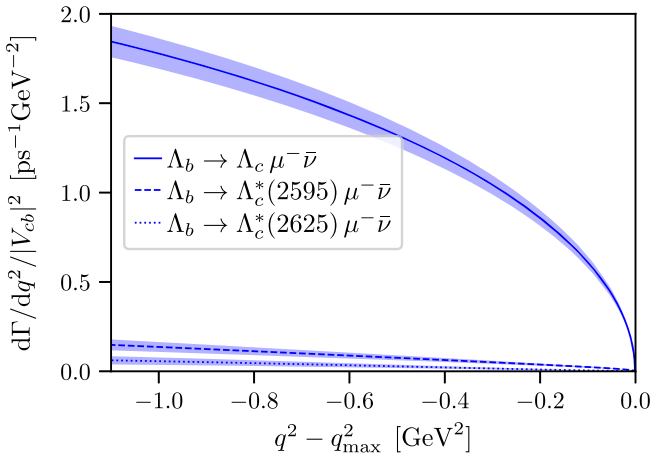

FIG. 9. Comparison of the $\Lambda_b \to \Lambda_c \mu^- \bar{\nu}$, $\Lambda_b \to \Lambda_c^*(2595)\mu^-\bar{\nu}$, and $\Lambda_b \to \Lambda_c^*(2625)\mu^-\bar{\nu}$ differential decay rates just below $q^2_{\rm max}$, calculated in the Standard Model using the form factors from lattice QCD.

latter. For example, at $q^2 = q^2_{\rm max} - 1\ {\rm GeV}^2$, the $\Lambda_b \to \Lambda_c^*(2595)\mu^-\bar{\nu}$ differential decay rate is approximately 13 times smaller than the $\Lambda_b \to \Lambda_c \mu^- \bar{\nu}$ differential decay rate.

IX. CONCLUSIONS

The decays $\Lambda_b \to \Lambda_c^*(2595)\ell^-\bar{\nu}$ and $\Lambda_b \to \Lambda_c^*(2625)\ell^-\bar{\nu}$ are interesting processes that deserve to be studied in detail, both experimentally and theoretically, to obtain a more complete picture of $b \to c\ell^-\bar{\nu}$ semileptonic decays. This work contributes to this goal by providing the first lattice-QCD determination of the complete set of form factors, albeit only in the vicinity of $q^2_{\rm max}$. The calculation was made possible by the technology developed initially for $\Lambda_b \to \Lambda^*(1520)$ [38]: working in the rest frame of the Λ_c^* to avoid mixing with unwanted quantum numbers, and using an interpolating field with gauge-covariant spatial derivatives to obtain a good overlap with the Λ_c^*.

In nature, the $\Lambda_c^*(2595)$ and $\Lambda_c^*(2625)$ are narrow resonances decaying through the strong interaction to $\Lambda_c\pi\pi$, with widths of $2.6(0.6)$ MeV and < 0.97 MeV, respectively [23]. These values justify the use of the narrow-width approximation. In our lattice calculation with three different pion masses in the range from approximately 300 to 430 MeV, we find that the Λ_c^* masses are below all possible strong-decay thresholds, including $\Sigma_c\pi$, except perhaps at the lowest pion mass. Simple chiral-continuum extrapolations of our lattice results for $m_{\Lambda_c^*(2595)}$ and $m_{\Lambda_c^*(2625)}$ yield values in agreement with experiment once systematic uncertainties are taken into account. The hyperfine splittings $m_{\Lambda_c^*(2625)} - m_{\Lambda_c^*(2595)}$ are also found to be consistent with experiment.

We use helicity-based definitions of the $\Lambda_b \to \Lambda_c^*(2595)$ and $\Lambda_b \to \Lambda_c^*(2625)$ form factors. On each ensemble we performed calculations for two different Λ_b momenta corresponding to $w \approx 1.01$ and $w \approx 1.03$, where $w = v \cdot v'$. The final results for the form factors, obtained from extrapolations to the continuum limit and physical pion mass, are parametrized as linear functions of w. These parametrizations are expected to be accurate only near the kinematic region where we have lattice data. Our results for the form factors at $w = 1$ are compatible (albeit only marginally in the case of the vector form factors) with the zero-recoil sum rules given in Ref. [25]. It will also be interesting to see the impact on unitarity bounds in global analyses of $b \to c\ell^-\bar{\nu}$ form factors [26].

Using our form-factor results, we evaluated the $\Lambda_b \to \Lambda_c^*(2595)\ell^-\bar{\nu}$ and $\Lambda_b \to \Lambda_c^*(2625)\ell^-\bar{\nu}$ differential decay rates, forward-backward asymmetry, and flat term in the Standard Model. We find the $\Lambda_b \to \Lambda_c^*(2595)\ell^-\bar{\nu}$ rates to be approximately 2.5 times higher than the $\Lambda_b \to \Lambda_c^*(2625)\ell^-\bar{\nu}$ rates (in the kinematic region considered), which is opposite to the behavior predicted by leading-order HQET but consistent with the expectation that subleading contributions in HQET are important for these types of decays. While not discussed in detail in this paper, we also attempted HQET fits at order $1/m$ [25,33] to our form factor results, but we did not obtain an acceptable description. We expect that $1/m^2$ corrections, which have not yet been studied for these processes, are also large. This will make it more challenging to combine experimental data for the shapes of the muonic decay rates in the entire kinematic range with the lattice results for the form factors near $q^2_{\rm max}$ to obtain Standard Model predictions for $R(\Lambda_c^*) = \mathcal{B}(\Lambda_b \to \Lambda_c^*\tau^-\bar{\nu})/\mathcal{B}(\Lambda_b \to \Lambda_c^*\mu^-\bar{\nu})$. Lattice calculations at lower q^2, while still working in the Λ_c^* rest frame, could be performed using finer lattices or using a moving-nonrelativistic QCD action [56] for the b quark. Alternatively, one could use nonzero Λ_c^* momenta and explicitly deal with the mixing of quantum numbers by extracting multiple states using larger operator bases, see for example Refs. [57,58].

ACKNOWLEDGMENTS

We thank Marzia Bordone and Danny van Dyk for discussions, and the RBC and UKQCD Collaborations for making their gauge field ensembles available. S. M. is supported by the U.S. Department of Energy, Office of Science, Office of High Energy Physics under Award No. DE-SC0009913. G. R. is supported by the U.S. Department of Energy, Office of Science, Office of Nuclear Physics, under Contract No. DE-SC0012704 (BNL). The computations for this work were carried out on facilities at the National Energy Research Scientific Computing Center, a DOE Office of Science User Facility supported by the Office of Science of the U.S. Department of Energy under Contract No. DE-AC02-05CH1123, and on facilities of the Extreme Science and Engineering Discovery Environment (XSEDE) [59], which is supported by National Science Foundation Grant No. ACI-1548562. We acknowledge the use of Chroma [60,61], QPhiX [62,63], QLUA [64], MDWF [65], and related USQCD software [66].

APPENDIX: RELATIONS BETWEEN DIFFERENT FORM FACTOR DEFINITIONS

In this Appendix, we provide expressions for the $\Lambda_b \to \Lambda_{c,1/2}^*$ and $\Lambda_b \to \Lambda_{c,3/2}^*$ form factors in other definitions used in the literature (for the vector and axial-vector currents only) in terms of our form factors. Note that the overall sign of the form factors for each decay mode depends on the phase conventions of the states. Thus, in the following relations, only the relative signs among the form factors for a specific final state are well determined. To make this explicit, we introduce factors of $\sigma^{(J^P)}$ below, which can take on the values ± 1.

1. Definition used by Leibovich and Stewart as well as Pervin, Roberts, and Capstick

We find that the $\Lambda_b \to \Lambda_{c,1/2}^*$ form factor definitions in Ref. [33] are related to ours as

$$d_{V_1} = \sigma_{\rm LS}^{(\frac{1}{2}^-)} f_\perp^{(\frac{1}{2}^-)}, \tag{A1}$$

$$d_{V_2} = -\sigma_{\rm LS}^{(\frac{1}{2}^-)} m_{\Lambda_b}\left[\frac{m_{\Lambda_b}+m_{\Lambda_{c,1/2}^*}}{q^2} f_0^{(\frac{1}{2}^-)} + \frac{m_{\Lambda_b}-m_{\Lambda_{c,1/2}^*}}{s_-}\left(1-\frac{m_{\Lambda_b}^2-m_{\Lambda_{c,1/2}^*}^2}{q^2}\right) f_+^{(\frac{1}{2}^-)} + \frac{2m_{\Lambda_{c,1/2}^*}}{s_-} f_\perp^{(\frac{1}{2}^-)}\right], \tag{A2}$$

$$d_{V_3} = -\sigma_{\rm LS}^{(\frac{1}{2}^-)} m_{\Lambda_{c,1/2}^*}\left[-\frac{m_{\Lambda_b}+m_{\Lambda_{c,1/2}^*}}{q^2} f_0^{(\frac{1}{2}^-)} + \frac{m_{\Lambda_b}-m_{\Lambda_{c,1/2}^*}}{s_-}\left(1+\frac{m_{\Lambda_b}^2-m_{\Lambda_{c,1/2}^*}^2}{q^2}\right) f_+^{(\frac{1}{2}^-)} - \frac{2m_{\Lambda_b}}{s_-} f_\perp^{(\frac{1}{2}^-)}\right], \tag{A3}$$

$$d_{A_1} = \sigma_{\rm LS}^{(\frac{1}{2}^-)} g_\perp^{(\frac{1}{2}^-)}, \tag{A4}$$

$$d_{A_2} = -\sigma_{\rm LS}^{(\frac{1}{2}^-)} m_{\Lambda_b}\left[-\frac{m_{\Lambda_b}-m_{\Lambda_{c,1/2}^*}}{q^2} g_0^{(\frac{1}{2}^-)} - \frac{m_{\Lambda_b}+m_{\Lambda_{c,1/2}^*}}{s_+}\left(1-\frac{m_{\Lambda_b}^2-m_{\Lambda_{c,1/2}^*}^2}{q^2}\right) g_+^{(\frac{1}{2}^-)} + \frac{2m_{\Lambda_{c,1/2}^*}}{s_+} g_\perp^{(\frac{1}{2}^-)}\right], \tag{A5}$$

$$d_{A_3} = -\sigma_{\rm LS}^{(\frac{1}{2}^-)} m_{\Lambda_{c,1/2}^*}\left[\frac{m_{\Lambda_b}-m_{\Lambda_{c,1/2}^*}}{q^2} g_0^{(\frac{1}{2}^-)} - \frac{m_{\Lambda_b}+m_{\Lambda_{c,1/2}^*}}{s_+}\left(1+\frac{m_{\Lambda_b}^2-m_{\Lambda_{c,1/2}^*}^2}{q^2}\right) g_+^{(\frac{1}{2}^-)} + \frac{2m_{\Lambda_b}}{s_+} g_\perp^{(\frac{1}{2}^-)}\right]. \tag{A6}$$

For $\Lambda_b \to \Lambda_{c,3/2}^*$, we find

$$l_{V_1} = \sigma_{\rm LS}^{(\frac{3}{2}^-)} \frac{m_{\Lambda_b} m_{\Lambda_{c,3/2}^*}}{s_-}[f_\perp^{(\frac{3}{2}^-)} + f_{\perp'}^{(\frac{3}{2}^-)}], \tag{A7}$$

$$\begin{aligned} l_{V_2} = \sigma_{\rm LS}^{(\frac{3}{2}^-)} \frac{m_{\Lambda_b}^2 m_{\Lambda_{c,3/2}^*}}{q^2 s_+ s_-}[&(m_{\Lambda_b}-m_{\Lambda_{c,3/2}^*}) s_- f_0^{(\frac{3}{2}^-)} - 2m_{\Lambda_{c,3/2}^*} q^2 (f_\perp^{(\frac{3}{2}^-)} - f_{\perp'}^{(\frac{3}{2}^-)}) \\ &- (m_{\Lambda_b}+m_{\Lambda_{c,3/2}^*})(m_{\Lambda_b}^2 - m_{\Lambda_{c,3/2}^*}^2 - q^2) f_+^{(\frac{3}{2}^-)}], \end{aligned} \tag{A8}$$

$$\begin{aligned} l_{V_3} = \sigma_{\rm LS}^{(\frac{3}{2}^-)} \frac{m_{\Lambda_b} m_{\Lambda_{c,3/2}^*}}{q^2 s_+ s_-}[&-m_{\Lambda_{c,3/2}^*}(m_{\Lambda_b}-m_{\Lambda_{c,3/2}^*}) s_- f_0^{(\frac{3}{2}^-)} - 2m_{\Lambda_b} m_{\Lambda_{c,3/2}^*} q^2 f_\perp^{(\frac{3}{2}^-)} + 2q^2 (m_{\Lambda_b} m_{\Lambda_{c,3/2}^*} - s_+) f_{\perp'}^{(\frac{3}{2}^-)} \\ &+ m_{\Lambda_{c,3/2}^*}(m_{\Lambda_b}+m_{\Lambda_{c,3/2}^*})(m_{\Lambda_b}^2 - m_{\Lambda_{c,3/2}^*}^2 + q^2) f_+^{(\frac{3}{2}^-)}], \end{aligned} \tag{A9}$$

$$l_{V_4} = \sigma_{\rm LS}^{(\frac{3}{2}^-)} f_{\perp'}^{(\frac{3}{2}^-)}, \tag{A10}$$

$$l_{A_1} = \sigma_{\rm LS}^{(\frac{3}{2}^-)} \frac{m_{\Lambda_b} m_{\Lambda_{c,3/2}^*}}{s_+}[g_\perp^{(\frac{3}{2}^-)} + g_{\perp'}^{(\frac{3}{2}^-)}], \tag{A11}$$

$$\begin{aligned} l_{A_2} = \sigma_{\rm LS}^{(\frac{3}{2}^-)} \frac{m_{\Lambda_b}^2 m_{\Lambda_{c,3/2}^*}}{q^2 s_+ s_-}[&-(m_{\Lambda_b}+m_{\Lambda_{c,3/2}^*}) s_+ g_0^{(\frac{3}{2}^-)} - 2m_{\Lambda_{c,3/2}^*} q^2 (g_\perp^{(\frac{3}{2}^-)} - g_{\perp'}^{(\frac{3}{2}^-)}) \\ &+ (m_{\Lambda_b}-m_{\Lambda_{c,3/2}^*})(m_{\Lambda_b}^2 - m_{\Lambda_{c,3/2}^*}^2 - q^2) g_+^{(\frac{3}{2}^-)}], \end{aligned} \tag{A12}$$

$$l_{A_3} = \sigma_{\mathrm{LS}}^{(\frac{3}{2}^-)} \frac{m_{\Lambda_b} m_{\Lambda^*_{c,3/2}}}{q^2 s_+ s_-} [m_{\Lambda^*_{c,3/2}} (m_{\Lambda_b} + m_{\Lambda^*_{c,3/2}}) s_+ g_0^{(\frac{3}{2}^-)} + 2 m_{\Lambda_b} m_{\Lambda^*_{c,3/2}} q^2 g_\perp^{(\frac{3}{2}^-)} - 2q^2 (m_{\Lambda_b} m_{\Lambda^*_{c,3/2}} + s_-) g_{\perp'}^{(\frac{3}{2}^-)}$$
$$- m_{\Lambda^*_{c,3/2}} (m_{\Lambda_b} - m_{\Lambda^*_{c,3/2}}) (m_{\Lambda_b}^2 - m_{\Lambda^*_{c,3/2}}^2 + q^2) g_+^{(\frac{3}{2}^-)}], \tag{A13}$$

$$l_{A_4} = \sigma_{\mathrm{LS}}^{(\frac{3}{2}^-)} g_{\perp'}^{(\frac{3}{2}^-)}. \tag{A14}$$

Pervin, Roberts, and Capstick [34] use the same definitions as Leibovich and Stewart, with the name replacements $d_{V_i} \to F_i$, $d_{A_i} \to G_i$ for the $\frac{1}{2}^-$ final state and $l_{V_i} \to F_i$, $l_{A_i} \to G_i$ for the $\frac{3}{2}^-$ final state.

2. Definition used by Gutsche *et al.*

We find that the form factor definitions used in Refs. [35,36] are related to ours as follows:

$$F_1^{V(\frac{1}{2}^-)} = \sigma_{\mathrm{G}}^{(\frac{1}{2}^-)} \frac{(m_{\Lambda_b} - m_{\Lambda^*_{c,1/2}})^2 (f_\perp^{(\frac{1}{2}^-)} - f_+^{(\frac{1}{2}^-)})}{s_-} - f_\perp^{(\frac{1}{2}^-)}, \tag{A15}$$

$$F_2^{V(\frac{1}{2}^-)} = \sigma_{\mathrm{G}}^{(\frac{1}{2}^-)} \frac{m_{\Lambda_b} (m_{\Lambda_b} - m_{\Lambda^*_{c,1/2}}) (f_\perp^{(\frac{1}{2}^-)} - f_+^{(\frac{1}{2}^-)})}{s_-}, \tag{A16}$$

$$F_3^{V(\frac{1}{2}^-)} = \sigma_{\mathrm{G}}^{(\frac{1}{2}^-)} \frac{m_{\Lambda_b} (m_{\Lambda_b} + m_{\Lambda^*_{c,1/2}}) (s_- f_0^{(\frac{1}{2}^-)} + q^2 f_\perp^{(\frac{1}{2}^-)} - (m_{\Lambda_b} - m_{\Lambda^*_{c,1/2}})^2 f_+^{(\frac{1}{2}^-)})}{q^2 s_-}, \tag{A17}$$

$$F_1^{A(\frac{1}{2}^-)} = \sigma_{\mathrm{G}}^{(\frac{1}{2}^-)} \frac{(m_{\Lambda_b} + m_{\Lambda^*_{c,1/2}})^2 (g_\perp^{(\frac{1}{2}^-)} - g_+^{(\frac{1}{2}^-)})}{s_+} - g_\perp^{(\frac{1}{2}^-)}, \tag{A18}$$

$$F_2^{A(\frac{1}{2}^-)} = -\sigma_{\mathrm{G}}^{(\frac{1}{2}^-)} \frac{m_{\Lambda_b} (m_{\Lambda_b} + m_{\Lambda^*_{c,1/2}}) (g_\perp^{(\frac{1}{2}^-)} - g_+^{(\frac{1}{2}^-)})}{s_+}, \tag{A19}$$

$$F_3^{A(\frac{1}{2}^-)} = \sigma_{\mathrm{G}}^{(\frac{1}{2}^-)} \frac{m_{\Lambda_b} (m_{\Lambda_b} - m_{\Lambda^*_{c,1/2}}) (-s_+ g_0^{(\frac{1}{2}^-)} - q^2 g_\perp^{(\frac{1}{2}^-)} + (m_{\Lambda_b} + m_{\Lambda^*_{c,1/2}})^2 g_+^{(\frac{1}{2}^-)})}{q^2 s_+}, \tag{A20}$$

$$F_1^{V(\frac{3}{2}^-)} = \sigma_{\mathrm{G}}^{(\frac{3}{2}^-)} f_{\perp'}^{(\frac{3}{2}^-)}, \tag{A21}$$

$$F_2^{V(\frac{3}{2}^-)} = \sigma_{\mathrm{G}}^{(\frac{3}{2}^-)} \frac{m_{\Lambda_b} m_{\Lambda^*_{c,3/2}}}{s_-} [f_\perp^{(\frac{3}{2}^-)} + f_{\perp'}^{(\frac{3}{2}^-)}], \tag{A22}$$

$$F_3^{V(\frac{3}{2}^-)} = \sigma_{\mathrm{G}}^{(\frac{3}{2}^-)} \frac{2 m_{\Lambda_b}^2}{s_- s_+} [-m_{\Lambda^*_{c,3/2}} (m_{\Lambda_b} + m_{\Lambda^*_{c,3/2}}) f_\perp^{(\frac{3}{2}^-)} + m_{\Lambda^*_{c,3/2}} (m_{\Lambda_b} + m_{\Lambda^*_{c,3/2}}) (f_{\perp'}^{(\frac{3}{2}^-)} + f_+^{(\frac{3}{2}^-)}) - s_+ f_{\perp'}^{(\frac{3}{2}^-)}], \tag{A23}$$

$$F_4^{V(\frac{3}{2}^-)} = \sigma_{\mathrm{G}}^{(\frac{3}{2}^-)} \frac{m_{\Lambda_b}^2 m_{\Lambda^*_{c,3/2}}}{q^2 s_+ s_-} [(m_{\Lambda_b} - m_{\Lambda^*_{c,3/2}}) s_- f_0^{(\frac{3}{2}^-)} - 2 m_{\Lambda^*_{c,3/2}} q^2 (f_\perp^{(\frac{3}{2}^-)} - f_{\perp'}^{(\frac{3}{2}^-)}),$$
$$- (m_{\Lambda_b} + m_{\Lambda^*_{c,3/2}}) (m_{\Lambda_b}^2 - m_{\Lambda^*_{c,3/2}}^2 - q^2) f_+^{(\frac{3}{2}^-)}], \tag{A24}$$

$$F_1^{A(\frac{3}{2}^-)} = \sigma_{\mathrm{G}}^{(\frac{3}{2}^-)} g_{\perp'}^{(\frac{3}{2}^-)} \tag{A25}$$

$$F_2^{A(\frac{3}{2}^-)} = \sigma_{\mathrm{G}}^{(\frac{3}{2}^-)} \frac{m_{\Lambda_b} m_{\Lambda^*_{c,3/2}}}{s_+} [g_\perp^{(\frac{3}{2}^-)} + g_{\perp'}^{(\frac{3}{2}^-)}], \tag{A26}$$

$$F_3^{A(\frac{3}{2}^-)} = \sigma_{\rm G}^{(\frac{3}{2}^-)} \frac{2m_{\Lambda_b}^2}{s_- s_+} [m_{\Lambda^*_{c,3/2}}(m_{\Lambda_b} - m_{\Lambda^*_{c,3/2}})(g_\perp^{(\frac{3}{2}^-)} - g_{\perp'}^{(\frac{3}{2}^-)} - g_+^{(\frac{3}{2}^-)}) - s_- g_{\perp'}^{(\frac{3}{2}^-)}], \tag{A27}$$

$$F_4^{A(\frac{3}{2}^-)} = \sigma_{\rm G}^{(\frac{3}{2}^-)} \frac{m_{\Lambda_b}^2 m_{\Lambda^*_{c,3/2}}}{q^2 s_+ s_-} [-(m_{\Lambda_b} + m_{\Lambda^*_{c,3/2}}) s_+ g_0^{(\frac{3}{2}^-)} - 2m_{\Lambda^*_{c,3/2}} q^2 (g_\perp^{(\frac{3}{2}^-)} - g_{\perp'}^{(\frac{3}{2}^-)}),$$
$$+ (m_{\Lambda_b} - m_{\Lambda^*_{c,3/2}})(m_{\Lambda_b}^2 - m_{\Lambda^*_{c,3/2}}^2 - q^2) g_+^{(\frac{3}{2}^-)}]. \tag{A28}$$

3. Definition used by Böer *et al.*

Reference [25] also uses a helicity-based definition, which we find to be related to ours as

$$f_{1/2,t} = \sigma_{\rm B}^{(\frac{1}{2}^-)} \frac{1}{2} \sqrt{\frac{3s_-}{m_{\Lambda_b} m_{\Lambda^*_{c,1/2}}}} \frac{m_{\Lambda_b} + m_{\Lambda^*_{c,1/2}}}{m_{\Lambda_b} - m_{\Lambda^*_{c,1/2}}} f_0^{(\frac{1}{2}^-)}, \tag{A29}$$

$$f_{1/2,0} = \sigma_{\rm B}^{(\frac{1}{2}^-)} \frac{1}{2} \sqrt{\frac{3s_+}{m_{\Lambda_b} m_{\Lambda^*_{c,1/2}}}} \frac{m_{\Lambda_b} - m_{\Lambda^*_{c,1/2}}}{m_{\Lambda_b} + m_{\Lambda^*_{c,1/2}}} f_+^{(\frac{1}{2}^-)}, \tag{A30}$$

$$f_{1/2,\perp} = \sigma_{\rm B}^{(\frac{1}{2}^-)} \frac{1}{2} \sqrt{\frac{3s_+}{m_{\Lambda_b} m_{\Lambda^*_{c,1/2}}}} f_\perp^{(\frac{1}{2}^-)}, \tag{A31}$$

$$g_{1/2,t} = \sigma_{\rm B}^{(\frac{1}{2}^-)} \frac{1}{2} \sqrt{\frac{3s_+}{m_{\Lambda_b} m_{\Lambda^*_{c,1/2}}}} \frac{m_{\Lambda_b} - m_{\Lambda^*_{c,1/2}}}{m_{\Lambda_b} + m_{\Lambda^*_{c,1/2}}} g_0^{(\frac{1}{2}^-)}, \tag{A32}$$

$$g_{1/2,0} = \sigma_{\rm B}^{(\frac{1}{2}^-)} \frac{1}{2} \sqrt{\frac{3s_-}{m_{\Lambda_b} m_{\Lambda^*_{c,1/2}}}} \frac{m_{\Lambda_b} + m_{\Lambda^*_{c,1/2}}}{m_{\Lambda_b} - m_{\Lambda^*_{c,1/2}}} g_+^{(\frac{1}{2}^-)}, \tag{A33}$$

$$g_{1/2,\perp} = \sigma_{\rm B}^{(\frac{1}{2}^-)} \frac{1}{2} \sqrt{\frac{3s_-}{m_{\Lambda_b} m_{\Lambda^*_{c,1/2}}}} g_\perp^{(\frac{1}{2}^-)}, \tag{A34}$$

$$F_{(1/2,t)} = \sigma_{\rm B}^{(\frac{3}{2}^-)} \frac{1}{4} \sqrt{\frac{s_-}{m_{\Lambda_b} m_{\Lambda^*_{c,3/2}}}} f_0^{(\frac{3}{2}^-)}, \tag{A35}$$

$$F_{(1/2,0)} = \sigma_{\rm B}^{(\frac{3}{2}^-)} \frac{1}{4} \sqrt{\frac{s_+}{m_{\Lambda_b} m_{\Lambda^*_{c,3/2}}}} f_+^{(\frac{3}{2}^-)}, \tag{A36}$$

$$F_{(1/2,\perp)} = \sigma_{\rm B}^{(\frac{3}{2}^-)} \frac{1}{4} \sqrt{\frac{s_+}{m_{\Lambda_b} m_{\Lambda^*_{c,3/2}}}} f_\perp^{(\frac{3}{2}^-)}, \tag{A37}$$

$$F_{(3/2,\perp)} = -\sigma_{\rm B}^{(\frac{3}{2}^-)} \frac{1}{4} \sqrt{\frac{s_+}{m_{\Lambda_b} m_{\Lambda^*_{c,3/2}}}} f_{\perp'}^{(\frac{3}{2}^-)}, \tag{A38}$$

$$G_{(1/2,t)} = \sigma_{\rm B}^{(\frac{3}{2}^-)} \frac{1}{4} \sqrt{\frac{s_+}{m_{\Lambda_b} m_{\Lambda^*_{c,3/2}}}} g_0^{(\frac{3}{2}^-)}, \tag{A39}$$

$$G_{(1/2,0)} = \sigma_{\rm B}^{(\frac{3}{2}^-)} \frac{1}{4} \sqrt{\frac{s_-}{m_{\Lambda_b} m_{\Lambda^*_{c,3/2}}}} g_+^{(\frac{3}{2}^-)}, \tag{A40}$$

$$G_{(1/2,\perp)} = \sigma_{\rm B}^{(\frac{3}{2}^-)} \frac{1}{4} \sqrt{\frac{s_-}{m_{\Lambda_b} m_{\Lambda^*_{c,3/2}}}} g_\perp^{(\frac{3}{2}^-)}, \tag{A41}$$

$$G_{(3/2,\perp)} = \sigma_{\rm B}^{(\frac{3}{2}^-)} \frac{1}{4} \sqrt{\frac{s_-}{m_{\Lambda_b} m_{\Lambda^*_{c,3/2}}}} g_{\perp'}^{(\frac{3}{2}^-)}. \tag{A42}$$

We also independently derived the Eqs. (B6) of Ref. [25] (arXiv version 2) which give the relations of the $\Lambda_b \to \Lambda^*_{c,3/2}$ form factors as defined in Ref. [25] to the definition used by Leibovich and Stewart [33]. We agree with seven of the eight equations but find the opposite relative sign for $G_{1/2,0}$.

[1] P. Gambino *et al.*, Challenges in semileptonic B decays, Eur. Phys. J. C **80**, 966 (2020).

[2] S. Bifani, S. Descotes-Genon, A. Romero Vidal, and M.-H. Schune, Review of lepton universality tests in B decays, J. Phys. G **46**, 023001 (2019).

[3] F. U. Bernlochner, M. F. Sevilla, D. J. Robinson, and G. Wormser, Semitauonic b-hadron decays: A lepton flavor universality laboratory, arXiv:2101.08326.

[4] M. Neubert, Heavy quark symmetry, Phys. Rep. **245**, 259 (1994).

[5] W. Detmold, C. Lehner, and S. Meinel, $\Lambda_b \to p\ell^-\bar{\nu}_\ell$ and $\Lambda_b \to \Lambda_c\ell^-\bar{\nu}_\ell$ form factors from lattice QCD with relativistic heavy quarks, Phys. Rev. D **92**, 034503 (2015).

[6] R. Aaij *et al.* (LHCb Collaboration), Determination of the quark coupling strength $|V_{ub}|$ using baryonic decays, Nat. Phys. **11**, 743 (2015).

[7] R. Dutta, $\Lambda_b \to (\Lambda_c, p)\tau\nu$ decays within standard model and beyond, Phys. Rev. D **93**, 054003 (2016).

[8] X.-Q. Li, Y.-D. Yang, and X. Zhang, $\Lambda_b \to \mathbf{\Lambda}_c\tau\bar{\nu}_\tau$ decay in scalar and vector leptoquark scenarios, J. High Energy Phys. 02 (2017) 068.

[9] J. Albrecht, F. Bernlochner, M. Kenzie, S. Reichert, D. Straub, and A. Tully, Future prospects for exploring present day anomalies in flavour physics measurements with Belle II and LHCb, arXiv:1709.10308.

[10] A. Datta, S. Kamali, S. Meinel, and A. Rashed, Phenomenology of $\Lambda_b \to \Lambda_c\tau\bar{\nu}_\tau$ using lattice QCD calculations, J. High Energy Phys. 08 (2017) 131.

[11] S. Alioli, V. Cirigliano, W. Dekens, J. de Vries, and E. Mereghetti, Right-handed charged currents in the era of the Large Hadron Collider, J. High Energy Phys. 05 (2017) 086.

[12] A. Ray, S. Sahoo, and R. Mohanta, Probing new physics in semileptonic Λ_b decays, Phys. Rev. D **99**, 015015 (2019).

[13] P. Böer, A. Kokulu, J.-N. Toelstede, and D. van Dyk, Angular analysis of $\Lambda_b \to \Lambda_c(\to \Lambda\pi)\ell\bar{\nu}$, J. High Energy Phys. 12 (2019) 082.

[14] N. Penalva, E. Hernández, and J. Nieves, Further tests of lepton flavour universality from the charged lepton energy distribution in $b \to c$ semileptonic decays: The case of $\Lambda_b \to \Lambda_c\ell\bar{\nu}_\ell$, Phys. Rev. D **100**, 113007 (2019).

[15] M. Ferrillo, A. Mathad, P. Owen, and N. Serra, Probing effects of new physics in $\Lambda_b^0 \to \Lambda_c^+\mu^-\bar{\nu}_\mu$ decays, J. High Energy Phys. 12 (2019) 148.

[16] X.-L. Mu, Y. Li, Z.-T. Zou, and B. Zhu, Investigation of effects of new physics in $\Lambda_b \to \Lambda_c\tau\bar{\nu}_\tau$ decay, Phys. Rev. D **100**, 113004 (2019).

[17] Q.-Y. Hu, X.-Q. Li, Y.-D. Yang, and D.-H. Zheng, The measurable angular distribution of $\Lambda_b^0 \to \Lambda_c^+(\to \Lambda^0\pi^+)\tau^-(\to \pi^-\nu_\tau)\bar{\nu}_\tau$ decay, J. High Energy Phys. 02 (2021) 183.

[18] K. C. Bowler, R. D. Kenway, L. Lellouch, J. Nieves, O. Oliveira, D. G. Richards, C. T. Sachrajda, N. Stella, and P. Ueberholz (UKQCD Collaboration), First lattice study of semileptonic decays of Λ_b and Ξ_b baryons, Phys. Rev. D **57**, 6948 (1998).

[19] S. A. Gottlieb and S. Tamhankar, A lattice study of Λ_b semileptonic decay, Nucl. Phys. B, Proc. Suppl. **119**, 644 (2003).

[20] R. Aaij *et al.* (LHCb Collaboration), Measurement of the shape of the $\Lambda_b^0 \to \Lambda_c^+\mu^-\bar{\nu}_\mu$ differential decay rate, Phys. Rev. D **96**, 112005 (2017).

[21] F. U. Bernlochner, Z. Ligeti, D. J. Robinson, and W. L. Sutcliffe, New Predictions for $\Lambda_b \to \Lambda_c$ Semileptonic Decays and Tests of Heavy Quark Symmetry, Phys. Rev. Lett. **121**, 202001 (2018).

[22] F. U. Bernlochner, Z. Ligeti, D. J. Robinson, and W. L. Sutcliffe, Precise predictions for $\Lambda_b \to \Lambda_c$ semileptonic decays, Phys. Rev. D **99**, 055008 (2019).

[23] P. A. Zyla *et al.* (Particle Data Group Collaboration), Review of particle physics, Prog. Theor. Exp. Phys. **2020**, 083C01 (2020).

[24] T. Mannel and D. van Dyk, Zero-recoil sum rules for $\Lambda_b \to \Lambda_c$ form factors, Phys. Lett. B **751**, 48 (2015).

[25] P. Böer, M. Bordone, E. Graverini, P. Owen, M. Rotondo, and D. Van Dyk, Testing lepton flavour universality in semileptonic $\Lambda_b \to \Lambda_c^*$ decays, J. High Energy Phys. 06 (2018) 155.

[26] T. D. Cohen, H. Lamm, and R. F. Lebed, Precision model-independent bounds from global analysis of $b \to c\ell\nu$ form factors, Phys. Rev. D **100**, 094503 (2019).

[27] A. E. Blechman, A. F. Falk, D. Pirjol, and J. M. Yelton, Threshold effects in excited charmed baryon decays, Phys. Rev. D **67**, 074033 (2003).

[28] Z.-H. Guo and J. A. Oller, Resonance on top of thresholds: The $\Lambda_c(2595)^+$ as an extremely fine-tuned state, Phys. Rev. D **93**, 054014 (2016).

[29] A. J. Arifi, H. Nagahiro, and A. Hosaka, Three-body decay of $\Lambda_c^*(2595)$ and $\Lambda_c^*(2625)$ with the inclusion of a direct two-pion coupling, Phys. Rev. D **98**, 114007 (2018).

[30] J. Nieves, R. Pavao, and S. Sakai, Λ_b decays into $\Lambda_c^*\ell\bar{\nu}_\ell$ and $\Lambda_c^*\pi^-$ [$\Lambda_c^* = \Lambda_c(2595)$ and $\Lambda_c(2625)$] and heavy quark spin symmetry, Eur. Phys. J. C **79**, 417 (2019).

[31] J. Nieves and R. Pavao, Nature of the lowest-lying odd parity charmed baryon $\Lambda_c(2595)$ and $\Lambda_c(2625)$ resonances, Phys. Rev. D **101**, 014018 (2020).

[32] W. Roberts, Semileptonic decays of heavy Lambda's into excited baryons, Nucl. Phys. **B389**, 549 (1993).

[33] A. K. Leibovich and I. W. Stewart, Semileptonic Λ_b decay to excited Λ_c baryons at order $\Lambda_{\rm QCD}/m_Q$, Phys. Rev. D **57**, 5620 (1998).

[34] M. Pervin, W. Roberts, and S. Capstick, Semileptonic decays of heavy Λ baryons in a quark model, Phys. Rev. C **72**, 035201 (2005).

[35] T. Gutsche, M. A. Ivanov, J. G. Körner, V. E. Lyubovitskij, V. V. Lyubushkin, and P. Santorelli, Theoretical description of the decays $\Lambda_b \to \Lambda^{(*)}(\frac{1}{2}^\pm, \frac{3}{2}^\pm) + J/\psi$, Phys. Rev. D **96**, 013003 (2017).

[36] T. Gutsche, M. A. Ivanov, J. G. Körner, V. E. Lyubovitskij, P. Santorelli, and C.-T. Tran, Analyzing lepton flavor universality in the decays $\Lambda_b \to \Lambda_c^{(*)}(\frac{1}{2}^\pm, \frac{3}{2}^-) + \ell\bar{\nu}_\ell$, Phys. Rev. D **98**, 053003 (2018).

[37] D. Bečirević, A. Le Yaouanc, V. Morénas, and L. Oliver, Heavy baryon wave functions, Bakamjian-Thomas approach to form factors, and observables in $\Lambda_b \to \Lambda_c(\frac{1}{2}^\pm)\ell\bar{\nu}$ transitions, Phys. Rev. D **102**, 094023 (2020).

[38] S. Meinel and G. Rendon, $\Lambda_b \to \Lambda^*(1520)\ell^+\ell^-$ form factors from lattice QCD, Phys. Rev. D **103**, 074505 (2021).

[39] T. Feldmann and M. W. Y. Yip, Form factors for $\Lambda_b \to \Lambda$ transitions in the soft-collinear effective theory, Phys. Rev.

D **85**, 014035 (2012); Erratum, Phys. Rev. D **86**, 079901 (2012).
[40] Y. Aoki, N. H. Christ, J. M. Flynn, T. Izubuchi, C. Lehner, M. Li, H. Peng, A. Soni, R. S. Van de Water, and O. Witzel (RBC and UKQCD Collaborations), Nonperturbative tuning of an improved relativistic heavy-quark action with application to bottom spectroscopy, Phys. Rev. D **86**, 116003 (2012).
[41] Z. S. Brown, W. Detmold, S. Meinel, and K. Orginos, Charmed bottom baryon spectroscopy from lattice QCD, Phys. Rev. D **90**, 094507 (2014).
[42] Y. Aoki *et al.* (RBC and UKQCD Collaborations), Continuum limit physics from $2 + 1$ flavor domain wall QCD, Phys. Rev. D **83**, 074508 (2011).
[43] T. Blum *et al.* (RBC and UKQCD Collaborations), Domain wall QCD with physical quark masses, Phys. Rev. D **93**, 074505 (2016).
[44] T. Blum, T. Izubuchi, and E. Shintani, New class of variance-reduction techniques using lattice symmetries, Phys. Rev. D **88**, 094503 (2013).
[45] E. Shintani, R. Arthur, T. Blum, T. Izubuchi, C. Jung, and C. Lehner, Covariant approximation averaging, Phys. Rev. D **91**, 114511 (2015).
[46] R. C. Johnson, Angular momentum on a lattice, Phys. Lett. **114B**, 147 (1982).
[47] J. A. Oller and U. G. Meissner, Chiral dynamics in the presence of bound states: Kaon nucleon interactions revisited, Phys. Lett. B **500**, 263 (2001).
[48] S. Hashimoto, A. X. El-Khadra, A. S. Kronfeld, P. B. Mackenzie, S. M. Ryan, and J. N. Simone, Lattice QCD calculation of $\bar{B} \to D\ell\bar{\nu}$ decay form-factors at zero recoil, Phys. Rev. D **61**, 014502 (1999).
[49] A. X. El-Khadra, A. S. Kronfeld, P. B. Mackenzie, S. M. Ryan, and J. N. Simone, The semileptonic decays $B \to \pi\ell\nu$ and $D \to \pi\ell\nu$ from lattice QCD, Phys. Rev. D **64**, 014502 (2001).
[50] W. Detmold and S. Meinel, $\Lambda_b \to \Lambda\ell^+\ell^-$ form factors, differential branching fraction, and angular observables from lattice QCD with relativistic b quarks, Phys. Rev. D **93**, 074501 (2016).
[51] See Supplemental Material at http://link.aps.org/supplemental/10.1103/PhysRevD.103.094516, for files containing the form-factor parameter values and covariance matrices.
[52] M. A. Shifman, N. G. Uraltsev, and A. I. Vainshtein, $|V_{cb}|$ from OPE sum rules for heavy flavor transitions, Phys. Rev. D **51**, 2217 (1995); Erratum, Phys. Rev. D **52**, 3149 (1995).
[53] I. I. Y. Bigi, M. A. Shifman, N. G. Uraltsev, and A. I. Vainshtein, Sum rules for heavy flavor transitions in the SV limit, Phys. Rev. D **52**, 196 (1995).
[54] P. Gambino, T. Mannel, and N. Uraltsev, $B \to D^*$ at zero recoil revisited, Phys. Rev. D **81**, 113002 (2010).
[55] P. Gambino, T. Mannel, and N. Uraltsev, $B \to D^*$ zero-recoil formfactor and the heavy quark expansion in QCD: A systematic study, J. High Energy Phys. 10 (2012) 169.
[56] R. Horgan *et al.*, Moving NRQCD for heavy-to-light form factors on the lattice, Phys. Rev. D **80**, 074505 (2009).
[57] F. M. Stokes, W. Kamleh, D. B. Leinweber, M. S. Mahbub, B. J. Menadue, and B. J. Owen, Parity-expanded variational analysis for nonzero momentum, Phys. Rev. D **92**, 114506 (2015).
[58] G. Silvi *et al.*, P-wave nucleon-pion scattering amplitude in the $\Delta(1232)$ channel from lattice QCD, arXiv:2101.00689.
[59] J. Towns, T. Cockerill, M. Dahan, I. Foster, K. Gaither, A. Grimshaw, V. Hazlewood, S. Lathrop, D. Lifka, G. D. Peterson, R. Roskies, J. R. Scott, and N. Wilkins-Diehr, XSEDE: Accelerating scientific discovery, Comput. Sci. Eng. **16**, 62 (2014).
[60] R. G. Edwards and B. Joo (SciDAC LHPC, and UKQCD Collaborations), The Chroma software system for lattice QCD, Nucl. Phys. B, Proc. Suppl. **140**, 832 (2005).
[61] R. G. Edwards, B. Joó *et al.*, Chroma, https://github.com/JeffersonLab/chroma.
[62] B. Joó, M. Smelyanskiy, D. D. Kalamkar, and K. Vaidyanathan, Chapter 9—Wilson Dslash Kernel From Lattice QCD Optimization, in *High Performance Parallelism Pearls* (Morgan Kaufmann, Boston, 2015), pp. 139–170.
[63] B. Joó *et al.*, QPhiX Dslash and Solver Library, https://github.com/jeffersonlab/qphix.
[64] A. Pochinsky, S. Syritsyn *et al.*, QLUA, https://usqcd.lns.mit.edu/w/index.php/QLUA.
[65] A. Pochinsky, S. Syritsyn *et al.*, Möbius Domain Wall Inverter, https://github.com/usqcd-software/mdwf.
[66] USQCD Collaboration, USQCD Software, http://usqcd-software.github.io.